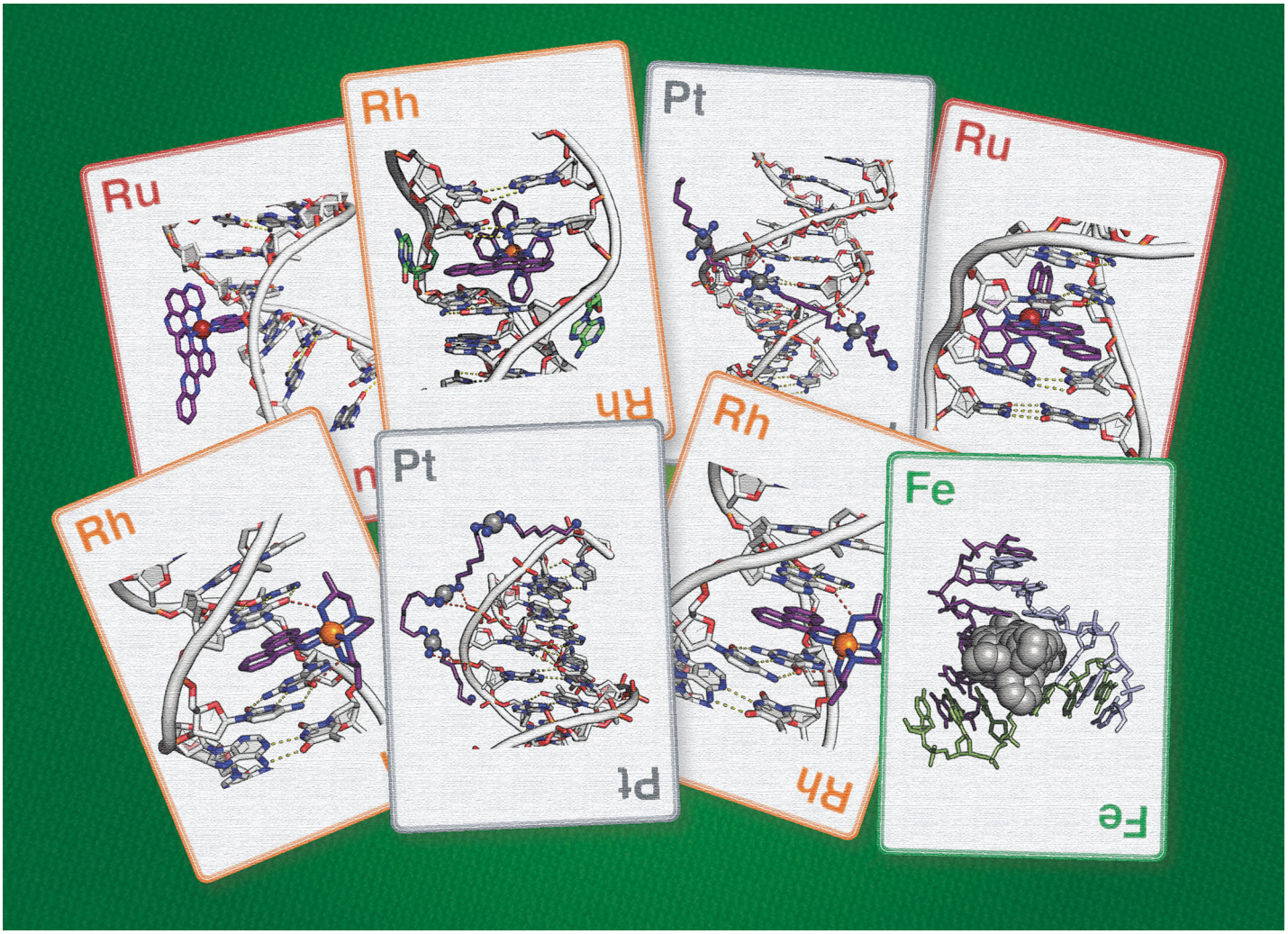

Featuring work from the research groups of Dr Andrew Kellett, Dublin City University, Ireland, and Dr Nicholas Farrell, Virginia Commonwealth University, US.

Molecular methods for assessment of non-covalent metallodrug–DNA interactions

We provide an accessible account of molecular methods to probe inorganic-nucleic acid interactions. Techniques are described using copper(II) and platinum(II) complexes prepared in our laboratories.

As featured in:

See Andrew Kellett, Nicholas P. Farrell *et al.*, *Chem. Soc. Rev.*, 2019, **48**, 971.

ROYAL SOCIETY OF CHEMISTRY | Celebrating IYPT 2019

rsc.li/chem-soc-rev

Registered charity number: 207890

Chem Soc Rev

TUTORIAL REVIEW

View Article Online
View Journal | View Issue

Cite this: *Chem. Soc. Rev.*, 2019, **48**, 971

Molecular methods for assessment of non-covalent metallodrug–DNA interactions

Andrew Kellett, *[a] Zara Molphy, [a] Creina Slator, [a] Vickie McKee [ab] and Nicholas P. Farrell *[c]

The binding of small molecule metallodrugs to discrete regions of nucleic acids is an important branch of medicinal chemistry and the nature of these interactions, allied with sequence selectivity, forms part of the backbone of modern medicinal inorganic chemistry research. In this tutorial review we describe a range of molecular methods currently employed within our laboratories to explore novel metallodrug–DNA interactions. At the outset, an introduction to DNA from a structural perspective is provided along with descriptions of non-covalent DNA recognition focusing on intercalation, insertion, and phosphate binding. Molecular methods, described from a non-expert perspective, to identify non-covalent and pre-associative nucleic acid recognition are then demonstrated using a variety of techniques including direct (non-optical) and indirect (optical) methods. Direct methods include: X-ray crystallography; NMR spectroscopy; mass spectrometry; and viscosity while indirect approaches detail: competitive inhibition experiments; fluorescence and absorbance spectroscopy; circular dichroism; and electrophoresis-based techniques. For each method described we provide an overview of the technique, a detailed examination of results obtained and relevant follow-on of advanced biophysical/analytical techniques. To achieve this, a selection of relevant copper(II) and platinum(II) complexes developed within our laboratories are discussed and are compared, where possible, to classical DNA binding agents. Applying these molecular methods enables us to determine structure–activity factors important to rational metallodrug design. In many cases, combinations of molecular methods are required to comprehensively elucidate new metallodrug–DNA interactions and, from a drug discovery perspective, coupling this data with cellular responses helps to inform understanding of how metallodrug–DNA binding interactions manifest cytotoxic action.

Received 20th August 2018

DOI: 10.1039/c8cs00157j

rsc.li/chem-soc-rev

Key learning points

- Essentials of nucleic acid structure.
- Principles of nucleic acid–metallodrug recognition.
- Application of mass spectrometry, nuclear magnetic resonance spectroscopy and X-ray crystallography to probe selective metallodrug–DNA binding sites.
- Quantification of metallodrug–DNA interactions using high-throughput optical techniques based on fluorescence and absorbance spectroscopy.
- Electrophoretic techniques and the use of on-chip microfluidic assays to identify drug–DNA damage.

1. An introduction to DNA structure and function.

1.1. DNA structure

Nucleic acids are a critical molecular target for candidate anti-tumoral metallodrugs. The electron-rich phosphate backbone, donor heteroatoms in the nucleobases, and intricate secondary and tertiary structures combine to create potential binding environments for both "free" metal ions and discrete complexes. From a medicinal chemistry perspective, the ability to probe metal complex coordination to DNA is essential for developing new architectures that selectively target oligonucleotides and specific oligonucleotide conformations. Furthermore, given the essentiality of the DNA double-helix for the storage of genetic information and thus mediation of faithful cell replication, the interruption of biogenesis at this juncture provides a basic target for metallodrug discovery.[1]

The biologically predominant B-form of duplex DNA comprises a right-handed double helix containing two antiparallel sugar-phosphate chains (Fig. 1A). The heteroaromatic bases lie

[a] *School of Chemical Sciences and the National Institute for Cellular Biotechnology, Dublin City University, Glasnevin, Dublin 9, Ireland. E-mail: andrew.kellett@dcu.ie; Tel: +353 1 7005461*
[b] *Department of Physics, Chemistry and Pharmacy, University of Southern Denmark, Campusvej 55, 5230 Odense M, Denmark*
[c] *Department of Chemistry, Virginia Commonwealth University, Richmond, VA 23284-2006, USA. E-mail: npfarrell@vcu.edu; Tel: +1 804 8286320*

in the centre of the helix and hydrogen bonding between them effectively binds the two helical chains together. This structure is supported by stacking interactions that orient the base pairs perpendicular to the helical axis. DNA bases follow Chargaff's rules whereby a 1 : 1 (purine : pyrimidine) relationship exists between A and T as well as G and C (Fig. 1B).[2] The angle between the glycosidic bonds and the hydrogen bonds results in unequal grooves in the helical structure referred to as the minor and major grooves. Structural characteristics of B-DNA can thus be exploited for molecular recognition as the major groove (10.5 Å) is wider than the minor groove (4.8 Å), although their depths are generally identical.[3] Between the base pairs of B-DNA there is an axial rise of 3.4 Å (0.34 nm) and a 34.5° twist angle associated with every residue rotation while the helix diameter is 20 Å (Fig. 1C). In B-DNA the 2′-deoxyribose ring exists in the C2′-*endo* twist conformation, in contrast to the C3′-*endo* twist conformation found within both A and Z-DNA (Fig. 1D).[4,5] Along with Watson–Crick (WC) base pairing, π–π stacking interactions provide additional stability to the double helix; the overlap between successive 5′ → 3′ bases differs significantly however as evidenced by the overlap of TA/TA and AT/AT steps shown in Fig. 1E.

The flexibility of DNA lends itself to the formation of many alternative conformations generated under the influence of solvent conditions and small molecules. A-DNA is the dehydrated form of B-DNA and has a similar but more rigid and compacted structure consisting of 11 base pairs per helical turn with a axial rise of 2.55 Å between bases pairs (Fig. 1A and C).[6] Z-DNA is formed during the transcription process *in vivo* due to the torsional strains generated as negative supercoils are created by RNA polymerase moving along the sequence of the DNA double helix. There is a radical difference between Z- and B-DNA as the helical sense flips from right- to left-handed; this conformational change is due to alternating *syn*- and *anti*-conformations of purine and pyrimidine bases, respectively. Structurally, Z-DNA is elongated and narrow with a diameter of 18 Å and is composed of a single narrow groove analogous to that of the minor groove of B-DNA resulting in a zigzag arrangement of the backbone (Fig. 1A).[5] Besides these "canonical forms" of DNA other forms of DNA such as triplexes, G-quadruplexes and I-motifs are important for gene-specific drug targeting.[7,8]

Significant effort has been expended in recent years to determine how metallodrug molecules interact with nucleic acids and a number of complementary molecular methods have been developed to probe reversible and non-reversible interactions. In the absence of high-resolution structural data from X-ray diffraction or NMR studies, the mode of binding must be

From left to right: Dr Zara Molphy, Dr Andrew Kellett, Prof. Nicholas P. Farrell, Dr Creina Slator, and Prof. Vickie McKee

Dr Andrew Kellett is a graduate of Maynooth University and Technological University Dublin. He is currently Associate Professor of Inorganic and Medicinal Chemistry at Dublin City University (DCU). His research intersects bioinorganic and nucleic acids research fields and his work is supported by Science Foundation Ireland (SFI), the Synthesis and Solid State Pharmaceutical Centre (SSPC), CÚRAM, the Irish Research Council (IRC), and the European Union's Horizon 2020 programme. The current focus of his group is centred on artificial gene editing and therapeutic nucleic acids.

Dr Zara Molphy completed her BSc in Chemical and Pharmaceutical Sciences at DCU, graduating with a first class honours degree in 2012. She was awarded an Irish Research Council (IRC) Postgraduate Scholarship in 2013 and received her PhD in the area of bioinorganic and nucleic acid chemistry under the supervision of Prof. Andrew Kellett in 2017. She is currently a postdoctoral researcher in the Science Foundation Ireland (SFI) funded polynuclear platinum biomaterials project with expertise in drug design, molecular biology, and DNA damage/repair.

Dr Creina Slator obtained her BSc in Chemical and Pharmaceutical Sciences (Hons) in 2012 at Dublin City University (DCU). She received her PhD in bioinorganic and medicinal chemistry in 2017 under the supervision of Prof. Andrew Kellett and was a recipient of a Distinguished Scholarship from DCU and also an Irish Research Council Scholarship. She is now a postdoctoral research fellow at DCU working in Science Foundation Ireland (SFI) funded research projects dedicated to platinum and copper biomaterials development.

Professor Vickie McKee obtained a PhD in macrocyclic chemistry from Queen's University, Belfast. She is currently Adjunkt Professor in Syddansk Universitet, Odense, Denmark and Adjunct Professor in Dublin City University. Her research interests are primarily in bioinorganic coordination chemistry and crystallography.

Professor Nicholas P. Farrell is a graduate of University College Dublin and Sussex University. He is currently Professor of Chemistry at Virginia Commonwealth University (VCU) where he was Distinguished Research Scholar for 2003–2004. Professor Farrell's activities are both highly interdisciplinary and international in scope. He and his collaborators have received over sixty patents world-wide from his inventions. He was Chair of the first Gordon Research Conference on Metals in Medicine in 2002. He is a 2010–2015 Jefferson Science Fellow and a Corresponding Member of the Brazilian Academy of Sciences.

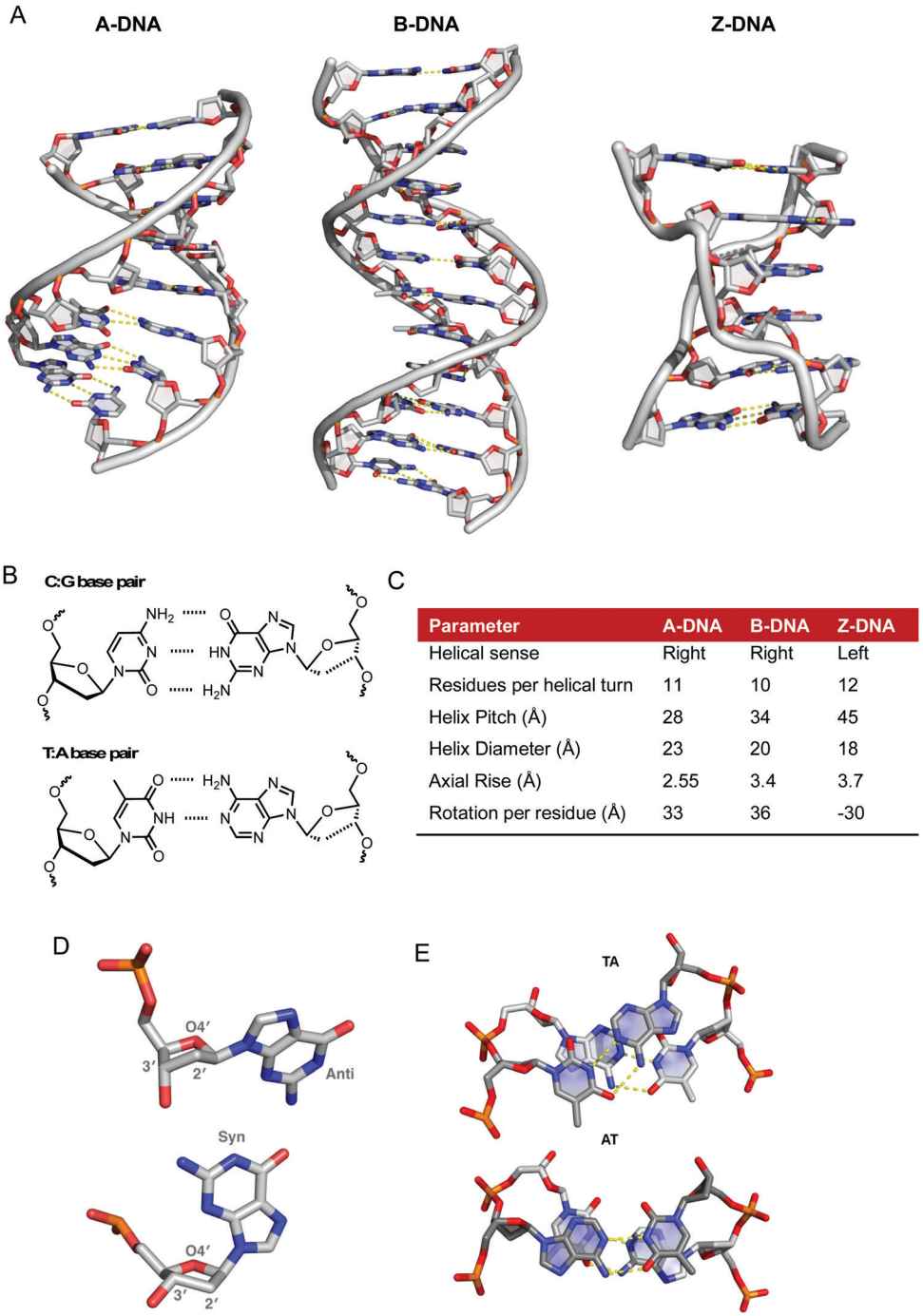

Fig. 1 (A) X-ray structures of A-, B- and Z-DNA from PDB files 1VJ4, 1BNA and 2DCG respectively, (B) hydrogen bonding between C–G and T–A base pairs, (C) summary of structural differences between A-, B- and Z-DNA;[6] (D) conformational preferences of the 2′-deoxyribose rings of DNA taken from 1BNA and 2DGC with respective *anti*- and *syn*-conformations of guanine nucleobase and (E) top down view of stacking interactions in TA and AT steps from PDB 167D (d(CCATTAATGG)$_2$). Hydrogen bonds are shown as dashed yellow lines; the angle between the vectors representing the two N3(T) → N1(A) hydrogen bonds is 118° for the TA step and 160° for the AT step.

inferred indirectly from molecular and biophysical solution studies. A wealth of information regarding the binding mode and sequence specificity of these interactions can be determined and in this tutorial review we provide an overview of selected molecular methods to identify metallodrug–DNA interactions with particular emphasis on copper(II) and platinum(II) complexes of current interest to our research programmes (*cf.* Fig. 2A–D). While much evidence has been accumulated on covalently bound adducts, the potential for sequence specificity is in some ways linked to the pre-association or ''non-covalent'' interactions occurring prior to covalent bond formation and these aspects are emphasized herein.

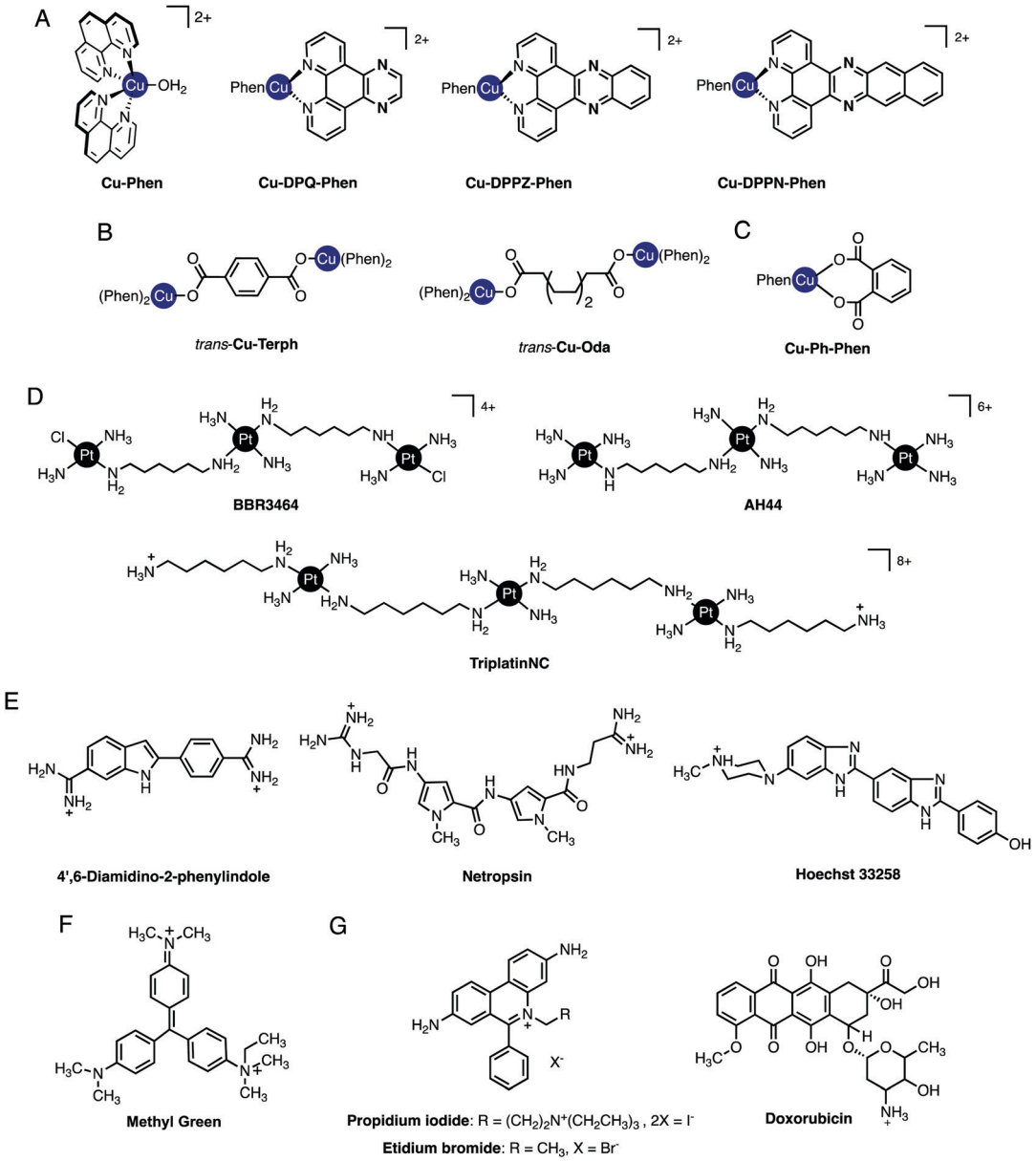

Fig. 2 (A) Cu-Phen and ternary copper(II) phenanthrene complexes Cu-DPQ-Phen, Cu-DPPZ-Phen and Cu-DPPN-Phen; (B) di-nuclear copper(II) terephthalate (Cu-Terph) and octanedioate (Cu-Oda) complexes; (C) square planar copper(II) complex Cu-Ph-Phen incorporating *o*-phthalate and 1,10-phenanthroline; (D) polynuclear platinum complexes (PPCs) $[\{trans\text{-}PtCl(NH_3)_2\}_2\text{-}\mu\text{-}\{trans\text{-}Pt(NH_3)_2(NH_2(CH_2)_6NH_2)_2\}]^{4+}$ (Triplatin, BBR3464), $[\{Pt(NH_3)_3\}_2\text{-}\mu\text{-}\{trans\text{-}Pt(NH_3)_2(NH_2(CH_2)_6NH_2)_2\}]^{6+}$ (AH44), and $[\{trans\text{-}Pt(NH_3)_2(NH_2(CH_2)_6NH_3)\}_2\text{-}\mu\text{-}(\{trans\text{-}Pt(NH_3)_2(NH_2(CH_2)_6NH_2)_2\})]^{8+}$ (TriplatinNC); and (E) Minor groove binding agents 4′,6-diamidino-2-phenylindole (DAPI), netropsin (Net), Hoechst 33258; (F) major groove binding methyl green (MG); and (G). planar heterocyclic intercalators propidium iodide (PI), ethidium bromide (EtBr) and doxorubicin (Dox).

1.2. Nucleic acids as metallodrug targets. Modes of binding by coordination and classical compounds

Non-covalent modes by which metal complexes bind to DNA include intercalation,[9,10] insertion,[11,12] groove binding,[13,14] and by discrete phosphate coordination such as the 'phosphate clamp'.[15] In all cases, structural factors based on the shape and charge of the complex underpin these binding modes and considerable effort is focused to uncover new inorganic scaffolds with selective and robust binding capability. The structural aspects of DNA are, of course, essential to the recognition process since they provide the template to which metal complexes bind. From a classical perspective, crescent-shaped organic molecules containing protonated terminal amines (*e.g.* netropsin and distamycin, Fig. 2E) are well-matched to the minor groove curvature and, once bound, give rise to helical contraction due to secondary non-covalent phosphate backbone-amine interactions.[16] Organic-based major groove binders, on the other hand, contain non-coplanar aromatic propeller-like conformations (*e.g.* methyl green, Fig. 2F) that bind due to hydrophobic interactions with the major groove floor with cationic amines located on the molecular periphery likely providing

ancillary stabilization.[17] In contrast to both major and minor groove binders, DNA intercalators (*e.g.* ethidium bromide) contain planar heteroaromatic structures, often with extended π-backbones, to facilitate penetration into the DNA backbone and subsequent van der Waals contacts between WC pairs (Fig. 2G).[18] The significance of these classical interactions to the discovery of new metallodrug–DNA binding modes and in proposing new metal complex-nucleic acid adducts is important to consider. Since classical binding modes are selective and in many cases structurally determined by primary techniques including X-ray structural analysis, comparisons using direct and indirect methods can be made between suspect metallodrug–DNA binding agents and suitable organic controls. In this tutorial review we take advantage of this approach and describe how classical agents can assist in uncovering drug–DNA interactions of novel agents.

2. Primary techniques

2.1. X-ray crystallography

Definitive visualization of coordination binding modes comes firstly from X-ray crystallography. Much of our current knowledge of detailed structural information is derived from X-ray crystallographic studies on single crystals of DNA, or oligonucleotides and their complexes with drug molecules. From the initial Franklin photographs demonstrating the helical nature of B-DNA in 1953,[19] through the conformational effects of cisplatin binding,[20] to more recent studies on intercalation, metalloinsertion and the phosphate clamp, crystallographic studies underpin our understanding of metallodrug–DNA structural chemistry. In recent years most biological macromolecular crystallography has been carried out at 3G synchrotron facilities where the availability of tunable, high intensity X-ray sources and fast, sensitive detectors has enabled study of ever smaller crystals at ever higher resolution.[21,22] At the same time, developments in laboratory instrumentation, notably microsource X-ray tubes and CCD or solid state detectors are arguably bringing small macromolecules such as nucleotide oligomers within range of laboratory sources.

Good quality data reveal a wealth of detailed, atomic-level structural information (and moderate quality data may also be very revealing). Essentially the experiment yields a 3D map of electron density from which the atomic positions are determined. Once the positions of the atoms are known, geometric data such as bond lengths and angles can be readily calculated and the structure can be explored and illustrated using graphics programs. For example, crystallographic data allow analysis of the hydrogen bonding responsible for the backbone-tracking phosphate clamp behaviour of TriplatinNC as shown in Fig. 2D as well as the stacking and hydrogen bonding involved in Δ-α-[Rh{(*R*,*R*)-Me_2trien}phi]$^{3+}$ intercalation (Fig. 3 and 4A).[12]

The main difficulty in using crystallography to study drug interactions with DNA or oligonucleotides is growing a good quality crystal of reasonable size. For this, a significant quantity of homogeneous, pure material is required and it may be necessary to test a wide range of conditions before a suitable set is found, so it may also be an expensive undertaking in terms of oligonucleotide materials.

2.1.1. Metallointercalation and metalloinsertion. Intercalation involves insertion of a planar, usually aromatic, ligand (or part thereof) between the stacked base pairs of DNA. This interaction was identified and characterised by Lerman in 1961 and many classes of organic intercalators have been recognized since.[23] Intercalation of metal complexes also has a long history, the first structurally characterized (from X-ray diffraction by fibres) example being the 2-hydroxyethanethiolato(2,2′,2′′-terpyridine)-platinum(II) monocation and a number of recent reviews have appeared describing intercalation by complexes of platinum, copper, ruthenium, rhodium and osmium.[10,12,24] The essential structural requirement is that the intercalating (or semi-intercalating) group must engage in base stacking interactions,

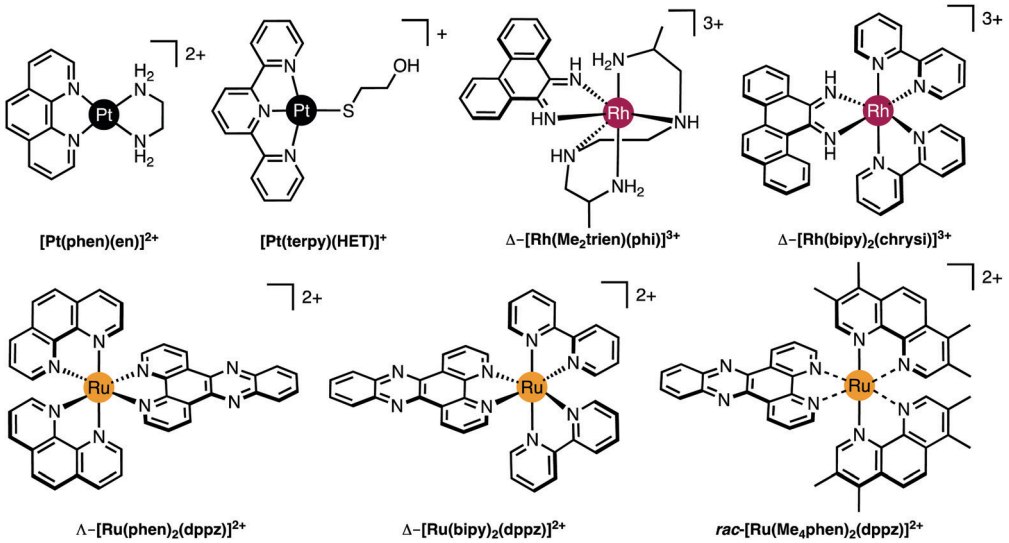

Fig. 3 Molecular structures of selected Pt(II), Rh(III) and Ru(II) intercalating and insertion complexes.

a major factor stabilising the DNA structure. The nature of "π-stacking" is complex and influenced by, for example, electrostatic substituent effects and solvent but generally requires both that the ligand is planar and that it contains a significant delocalized region. It is also necessary that the additional stabilisation on stacking the intercalating ligand outweighs the reorganization energy required to permit it. The intercalated groups orient approximately parallel to the plane of the base pairs, and the base pairing is not very significantly disturbed. The principal effect on the DNA structure is to extend it by *ca.* 3.6 Å for each intercalated group (3.6 Å being the normal interplanar distance for π-stacking). To permit this, the DNA helix unwinds, reducing the helical twist across the intercalation site. There are also a number of smaller geometric changes[20] that together may reduce conformational flexibility in the adjacent portions of the helix, since it is observed that further intercalation does not occur at the neighbouring sites (the "nearest neighbour exclusion principle").[25]

Since only the planar section of the ligand can intercalate, it needs to be large enough to achieve significant π-overlap, without bringing the remainder of the complex into unfavourable steric or electronic interaction. Ligands such as 1,10-phenanthroline (phen) and terpyridine (terpy) in square planar Pt complexes intercalate effectively but large ligands such as 9,10-phenanthrenequione diime (phi) or dipyridophenazine (dppz) are more effective for 6-coordinate complexes.[12] Recent examples of intercalation involving Ru(II) coordinated phen and TAP (1,4,5,8-tetra-aza-phenanthrene) ligands show partial intercalation that gives rise to DNA 'kinking' (Fig. 4D and PDB 4YMC).[10] The orientation of the intercalator in the "slot" between two base pairs may be symmetrical, or laterally offset relative to the principal axis of the DNA helix, presumably reflecting the best accessible set of stacking and other interactions, hence dependent on the detailed electronic structures of the intercalating ligand and the base pairs lining the intercalation site. There are ten possible intercalation sites,[25] differing in existing π-interactions between base pairs and their affinity for a specific intercalator. For example, in 1979 Lippard and co-workers showed that $[Pt(phen)(en)]^{2+}$ and $[Pt(terpy)(HET)]^{+}$ (where HET = 2-hydroxyethanethiolate) exhibit GC selectivity,[26] while $[Ru(phen)_2(dppz)]^{2+}$ (Fig. 3) displays preferential intercalation for poly-d(AT) over poly-d(GC).[12] The same complex intercalates symmetrically at the TA/TA step in $d(CCGGTACCGG)_2$ (Fig. 4C) but not the AT/AT site in $d(CCGGATCCGG)_2$.[10] In fact, many metallointercalators bind preferentially to DNA at specific sites, and this function can be amplified by interaction of the ancillary ligands with the DNA duplex. In an early example, the photoactive complex Δ-α-$[Rh\{(R,R)\text{-}Me_2trien\}phi]^{3+}$ (where Me_2trien = 2,9-diamino-4,7-diazadecane, Fig. 3) was found to specifically cleave the sequence 5′-TGCA-3′. The structural basis for this specificity was established by the X-ray structure of the complex bound to 5′-G(5|U)TGCAAC-3′ (Fig. 4A) in the major groove specifically at the 5′-TG|CA-3′ site (where | indicates phi insertion).[12] The intercalative π-stacking is supported by H-bonds from the amines of the Me_2trien ancillary ligands to the guanine-O6 acceptors as well as to some ordered water molecules.

Metalloinsertion is closely related to intercalation, also involving incorporation of a ligand into the base pair stack. The main difference is that in metalloinsertion one base pair is ejected and replaced by the incoming ligand. This interaction was predicted by Lerman but first structurally characterized in a metal complex only in 2007 for Δ-$[Rh(bpy)_2(chrysi)]^{3+}$ (where chrysi = 5,6-chrysenequinone diimine, Fig. 3 and 4B),[12] extended to a family of chrysi derivatives and more recently for both Δ-$[Ru(bipy)_2(dppz)]^{2+}$ and Λ-$[Ru(phen)_2(dppz)]^{2+}$ (where bipy = 2,2′-bipyridine, Fig. 3), in all three cases the insertion is at a mis-matched base pair and from the minor groove (in contrast to intercalation).[10,12] The dppz complexes are capable of both intercalation and insertion and it may be that other known intercalators are also capable of insertion in the presence of base-pair mismatches and perhaps matched base-pairs but evidence for this has yet to be established. Insertion involves less modification to

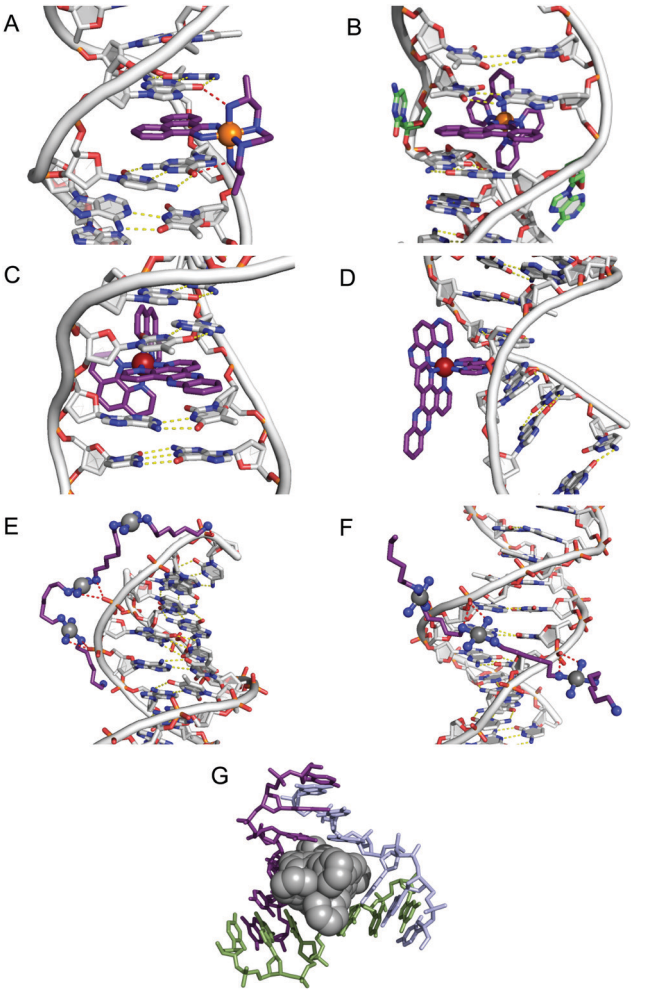

Fig. 4 Intercalation and insertion. (A) Δ-α-$[Rh\{(R,R)\text{-}Me_2trien\}phi]^{3+}$ intercalated into 5′-G(5|U)TGCAAC-3′ with additional stabilisation by H-bonds from the ancillary ligand (PDB 454d), black lines indicate hydrogen bonds and (B) Δ-$[Rh(bpy)_2(chrysi)]^{3+}$ inserted into (5′-CGGAAATTCCCG-3′), displacing a mismatched AC pair shown in green (PDB 2O1I) b; (C) intercalation of Λ-$[Ru(phen)_2(dppz)]^{2+}$ into $d(CCGGTACCGG)_2$ (PDB 3U38); (D) Λ-$[Ru(TAP)_2(dppz)]^{2+}$ bound to $d(CCGGATCCGG)_2$ by semi-intercalation (PDB 4YMC); TriplatinNC bound to Dickerson–Drew dodecamer (B-DNA) through backbone tracking (E) and groove spanning (F) interactions. (N–H···O=P hydrogen bonds shown as dashed red lines); and (G) three-way DNA junction recognition by a metallosupramolecular helicate $(Fe_2L_3)^{4+}$ where L = $C_{25}H_{20}N_4$ (PDB 2ET0).

the helical structure of DNA than intercalation. There is no significant extension or change in helicity although the "flipped out" bases are free to interact in other ways with the DNA helix or the inserting complex. The stabilisations due to hydrogen bonding of the displaced base pair and its stacking interactions are both lost and need to be replaced by the new π-stacking interactions (plus any new interactions involving the flipped out base pair). The relative contributions of base-stacking and base-pairing to DNA duplex stability depend on the particular sequence considered and, in some cases, the loss of the H-bonding component might not be expected to have a high cost. This is consistent with the observation that metalloinsertion can be specific for mismatched base pairs, especially those where the resulting base-pairing is energetically disfavoured (CC and CA). For example, Δ-$[Rh(bipy)_2(chrysi)]^{2+}$ (Fig. 3) can promote specific cleavage at a single mismatch site in a 2725 base pair linearized plasmid heteroduplex. This specificity is useful in detection of mismatches and is potentially diagnostic for cells with impaired mismatch repair (MMR) mechanisms; notably, a series of Rh-chrysi complexes that showed selective cytotoxicity for MMR-deficient cancer cells.[12]

As for intercalation, interaction of the ancillary ligands with DNA can be used to tune the binding properties of the inserting complex. For example, $[Ru(bipy)_2dppz]^{2+}$ binds to DNA *via* both intercalation and by insertion at mismatch sites but $[Ru(Me_4phen)_2(dppz)]^{2+}$ (where Me_4phen = 3,4,7,8-tetramethyl-1,10-phenanthroline, Fig. 3) is a mismatch-specific metallo-insertor where the methyl groups disfavour intercalation (due to steric interaction with the backbone) and also control the depth of dppz insertion.[12] As might be expected, the metalloinsertion correlates with the stability of the mismatch site, strongest for CC and CA (less stable), less striking for GG AA (more stable).

2.1.2. Non-covalent binding by polynuclear platinum complexes (PPCs): the phosphate clamp. One example of this structure is TriplatinNC designed with 'dangling' terminal hexanediamine ligands (Fig. 2D). The architecture of this complex gave rise to a previously undiscovered non-covalent DNA binding mode called the 'phosphate clamp' that results from am(m)ine-to-phosphate (N–H···O═P) hydrogen bonding directed through *cis*-oriented NH_3 (ammine) and -RNH_2 (amine) ligands.[27] The discrete mechanism of phosphate clamping gives rise to distinctive binding motifs: phosphate tracking and groove spanning (Fig. 4E and F). The groove spanning mode is dependent on helical topology localised to the minor groove and base sequence composition. These structures have been recently reviewed.[15]

2.1.3. Junction recognition by supramolecular cylinders. In contrast to intercalation and minor groove binding modes, Hannon and co-workers identified supramolecular di-iron(II) helicates recognise the major groove and stabilise 3-way DNA junctions.[13,28] Helicates of interest comprise a triple-stranded cylinder with *ca.* 2 nm length and 1 nm width thereby mimicking the major groove recognition unit of zinc fingers. In the presence of duplex DNA, efficient coiling was detected by AFM and it was later realised that helicate size appears more important than charge as increasing the dimensions by ~10% led to a significant reduction in coiling efficiency. Stabilisation of a 3-way palindromic junction of 5′-C**GTA**CG-3′ was established by X-ray crystallography (PDB 2ET0, Fig. 4G) where aside from electrostatic factors, aromatic surfaces of the cylinder π-stack with bases at the branch points of the junction. A 60° twist between π-stacking phenyl rings of the helicate matches the 60° kink in the DNA strand between T and A and this congruity appears central to 3-way junction recognition.

Method summary	DNA X-ray crystallography (direct)
Requirements	3G synchrotron facilities/microsource X-ray diffractometer.
Results	Definitive visualization of metallodrug–DNA binding interactions.
Advantages	Detailed structural data.
Limitations	Solid-state interactions only and transient/dynamic/pre-associative interactions may be precluded. Crystals of suitable quality required.
Complementary and advanced techniques	NMR and MS (direct) (Sections 2.2 and 2.3). CD/fluorescence/absorbance spectroscopy (indirect) (Sections 3.1 and 3.2). Advanced complementary methods include analysis by optical tweezers.

2.2. NMR studies

NMR studies complement the solid-state structures and give more information to the conformational variability in solution. NMR spectroscopy has benefitted significantly from advances in field strength, magnetic shielding and cryogenic probes. The most useful isotopes for NMR studies of platinum anticancer agents are ^1H, ^{15}N and ^{195}Pt. The latter is extremely sensitive to the nature of the ligands attached and can be used for speciation and kinetic studies. The use of $\{^1H,^{15}N\}$ HMQC/HSQC NMR spectroscopy greatly enhances sensitivity and is especially useful in kinetic studies with biological molecules.[29,30] Briefly, transfer of magnetization from the proton to a second heteronucleus such as ^{15}N gives a 2-dimensional spectrum with one axis for proton (^1H) and the other for ^{15}N, thus producing a spectrum with a peak for each unique proton attached to ^{15}N with the unique advantage of overcoming the inherent insensitivity of the ^{15}N nucleus. The sensitivity of the chemical shift and coupling constants (*e.g.* $^1J\{^{15}N–^{195}Pt\}$) to the nature of the *trans* ligands, and coupled to the fact that the only protons observed are those bound to the ^{15}N nucleus makes the technique of great practical use.[30] Pre-association and strong non-covalent binding can be observed as well as kinetics of DNA binding.

Cisplatin is a bifunctional DNA-binding agent which preferentially binds to N7 of guanine and adenine and typically results in 1,2-GG/AG intrastrand crosslinks with structural distortion through helical unwinding by 13°, and helical bending of 30–40° towards the major groove. It is generally accepted that aquation of cisplatin to give the more substitution-labile aquated species is necessary prior to covalent binding to DNA. Using $\{^1H,^{15}N\}$ HSQC NMR the stepwise aquation, monofunctional and

bifunctional nucleobase binding can be monitored and their respective rates of formation and equilibrium constants can be determined.[30]

When complexes with higher positive charge are concerned, pre-association with the biomolecule, and the effects of such pre-association on conformational preferences, can be observed. Triplatin (BBR3464, Fig. 2D) was the first multi-nuclear platinum complex to enter human clinical trials. The complex forms cross-linked bi-functional DNA adducts distinct from those of mono-nuclear species such as cisplatin. More specifically, the compound produces long-range inter- and intra-strand DNA platination and this behaviour is distinct from cisplatin's short range platination. A 3-fold slowing of the aquation of BBR3464 occurs in the presence of dsDNA but not ssDNA. This feature may account for the kinetic binding preference and may also be relevant in stabilization of G-quadruplex structures using BBR3464.[15] The results emphasize how the alteration of chemical properties of small molecules in the presence of large host interactions is dependent on the conformation and nature of that host and these examples show the utility of NMR techniques in probing these subtle interactions. Two examples are relevant to this tutorial:

(i) A unique feature of long-range {Pt,Pt} interstrand crosslinks is the occurrence of directional 5′ → 5′ and 3′ → 3′ isomers – the existence of the unusual 3′ → 3′ linkage isomer in the sequence was also confirmed by 2D NMR spectroscopy.[15,30] The initial orientation of BBR3464 on DNA mediated by electrostatic interactions transiently engaging with phosphate groups in the minor groove is an important feature which dictates not only isomer directionality but also the final conformation of covalently-bound interstrand crosslinks (1,4 *versus* 1,6) because in some cases the covalent adduct can be formed directly but in others, diffusion off the DNA is necessary for covalent binding to occur. These subtleties can be followed by 2D $\{^1H,^{15}N\}$ HSQC NMR.[30,31]

(ii) Using fully ^{15}N-labelled TriplatinNC, the presence of the phosphate clamp in solution with the Dickerson–Drew Duplex (DDD) was confirmed by observation of large chemical shift differences of the $\delta(NH_3)$ and $\delta(-NH_2R)$ in both the ^1H and ^{15}N dimensions.[32] The 2D $\{^1H,^{15}N\}$ HSQC NMR spectrum of ^{15}N-labeled TriplatinNC shows only two cross-peaks and a weak peak due to the dangling amine (Fig. 5). In the presence of DDD at pH 6, dramatic downfield ^{15}N shifts of approximately 20 ppm are observed, emphasising the dependency of shift on hybridization. The coupling constant changes are also consistent with formation of the phosphate clamp.[15]

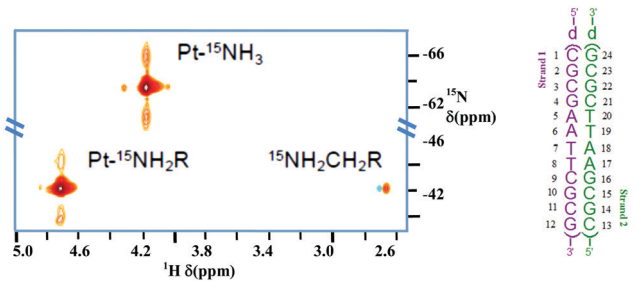

Fig. 5 $\{^1H,^{15}N\}$ HSQC NMR of TriplatinNC (left) and Dickerson–Drew Duplex (DDD, right). Satellites from $^1J(^{15}N-^{195}Pt)$ are clearly visible. Adapted with permission from Qu *et al.*[32] Reproduced from ref. 32 with permission from the Royal Society of Chemistry, copyright 2015.

Method summary	NMR analysis (direct)
Requirements	Good solubility. Labelled compounds (*e.g.* ^{15}N) best although natural abundance can be used in favourable circumstances.
Results	Conformation of metallodrug–DNA solution interactions.
Advantages	Modification of electronic properties of complex upon binding to oligonucleotide; kinetics of bond formation upon initial pre-association.
Limitations	Need NMR active nuclei and mainly diamagnetic compounds.
Complementary and advanced techniques	X-ray and MS (direct) (Sections 2.1 and 2.3). HSQC NMR can be combined with 3-D NOESY-HSQC or TOCSY-HSQC. Saturation transfer difference (STD) NMR to study transient complex-biomolecule interactions.

2.3. Mass spectrometry

Advances in technologies and ionization techniques now make Electrospray Ionization-Mass Spectrometry (ESI-MS) an indispensable tool for probing drug-nucleic acid interactions with several advantages; including the need for only a small sample, speed of use, and ease of analysis.[33] Covalent binding with biomolecules in general is easily observed and with appropriate digestion can pinpoint stoichiometry and binding sites of metallodrugs. It is in the study of non-covalent interactions where most interest resides because, if strong enough, the canonical non-covalent binding modes of hydrogen-bonding, electrostatic interactions, and intercalation can be transferred to the gas phase without disruption. Using appropriate non-denaturing conditions and carefully controlled instrumental optimization, electrospray ionization is able to transfer non-covalent complexes into the gas phase of the mass spectrometer without dissociation. Single-stranded, double-stranded and G-quadruplex DNA have all been studied and primary spectra combined with MS–MS techniques can give information on strength and sites of binding.[33]

ESI-MS has also proven useful in probing relative binding affinities of metal complexes to duplex and quadruplex DNA. Differences in binding within a series of octahedral metallo-intercalators based on $[Ru(phen)_3]^{2+}$ and $[Ru(phen)_2(dppz)]^{2+}$ and square-planar analogs such as $[Pt(en)(phen)]^{2+}$ demonstrated that the binding affinity in general towards quadruplex DNA is significantly less than that towards dsDNA.[33]

DNA as a template affects kinetics of substitution reactions occurring within its domain. Mass spectrometric studies using short 18-mer oligos showed a kinetic preference for binding of

BBR3464 to ssDNA over dsDNA. In this case, electrospray ionization coupled with Fourier transform ion cyclotron resonance mass spectrometry (ESI-FTICR-MS) is sufficiently sensitive to observe the 'pre-association' of the covalently binding molecule prior to Pt–DNA bond formation. For single-stranded DNA, the site of binding of the substitution-inert TriplatinNC and AH44 on a 18-mer ssDNA (5′-TCTCCCAGCGTGCGCCAT-3′) was ascertained using Tandem MS–MS of the 1 : 1 adducts (Fig. 6).[34] The binding is sufficiently strong that the fragment ion pattern is distinctly different and upon MS–MS there is no drug–DNA dissociation, only cleavage of the oligonucleotide backbone.

Full scan ESI-MS spectra of dsDNA AT duplex {5′-TAGCGC TTTTTCCGTA-3′}–{5′-TACGCGAAAAAGCGCTA-3′} complexed with substitution-inert PPCs also confirmed that the non-bonding interaction is strong enough to be transferred from solution to the gas phase. The CID spectra showed duplex unzipping into single strands with again no loss of PPC–DNA binding and duplex stabilization correlates with increasing charge and hydrogen bonding character of the complex. Upon increasing the collisional energy the single-stranded DNA formed dissociates as above.[29]

Method summary	Mass spectrometry (direct)
Requirements	Transfer to gas phase without bond cleavage.
Results	Covalent metallodrug–DNA binding interactions/binding stoichiometry/ non-covalent binding (gas phase).
Advantages	Very small quantities an advantage.
Limitation	Gas-phase results may not always translate to solution.
Complementary and advanced techniques	X-ray and NMR (direct) (Sections 2.1 and 2.2). High resolution CZE-MS, LA-ICP MS, and MALDI. Conformational preferences from ion-mobility studies.

2.4. Viscosity

Viscosity is a direct method where drug–DNA interactions are studied as a function of hydrodynamic changes induced by the binding agent. Experiments are carried out by introducing increasing ratios of drug to a solution containing a fixed concentration of DNA and observing how the velocity of DNA sedimentation influences a change in centipoise (cP). Relative viscosity data can be represented as (η/η_o) *versus* the [compound]/[DNA] ratio r, where η is the viscosity of complex treated DNA and η_o is the viscosity of untreated DNA. The technique is sensitive to changes in DNA chain length and individual modes of binding can be distinguished effectively since covalent and non-covalent binding modes display different hydrodynamic characteristics. Intercalators induce extension and unwinding of the DNA backbone due to separation of base pairs in order to accommodate the bound ligand. This results in the lengthening of the DNA molecule in proportion to the amount of drug bound (Fig. 7). The opposite effect can be noted for non-covalent major and minor groove binding agents since they cause little or no distortion to the phosphate backbone of DNA. In contrast, condensing agents such as the highly cationic TriplatinNC are capable of compacting and precipitating DNA that is indicated by a decreasing trend in viscosity relative to titrated complex (Fig. 7).[35] Cisplatin is also known to reduce viscosity since upon covalent binding it kinks the backbone which shortens the axis length of the DNA helix, thereby decreasing the relative viscosity. Since long-range coiling can impact viscosity measurements, high molecular weight DNA fibers can be sheared and examined in parallel to native experiments. We recently applied this approach with salmon testes DNA fibres and the Triplatin series to show sheared DNA fragments aggregate more efficiently due to increasing intramolecular phosphate clamping interactions on smaller nucleotide fragments.

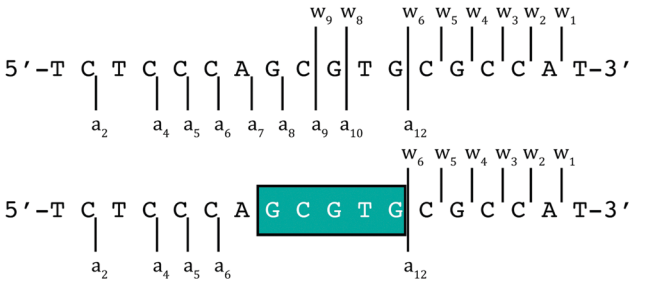

Fig. 6 ESI-MS/MS schematic of free (top) and PPC (either TriplatinNC or AH44) adducted (bottom) 5′-d(TCTCCCAGCGTGCGCCAT) at 100 and 120 V of collisional energy, respectively.[34] Fragmentation of the glycosidic bonds is prevalent throughout the free, with the region of enhanced stability in teal. The associated fragment ions (w_8^{2-}, w_9^{2-}, and a_9–a_{12} using standard McLuckey nomenclature) are absent in the adduct indicating the area of PPC binding.

Method summary	Viscosity (direct)
Requirements	Digital viscometer and polymeric nucleic acid sample (typically salmon testes/calf thymus DNA).
Results	Hydrodynamic (solution) phase modification to nucleic acids.
Advantages	Easy of use. Low cost. Suitable for bulk analysis.
Limitations	Compounds must result in changes to viscosity of DNA solution; minor groove binding compounds such as netropsin and pentamidine result in no change. Metal ions themselves can compact DNA (charge neutralization).
Complementary and advanced techniques	Optical techniques including thermal melting and circular dichroism (Sections 3.1.1 and 3.1.2). Gel based techniques including superhelical DNA unwinding and topoisomerase I-mediated DNA relaxation (Section 4.2). Advanced techniques include turbidity (UV), AFM, and DLS.

Compound	Mode of binding	η/η_o
EtBr	Intercalation	1.16
Actinomycin D	Threading intercalation	1.14
Netropsin	Minor groove	1.0
Pentamidine	Minor groove	0.99
$[Co(NH_3)_6]Cl_3$	Electrostatic	0.82
TriplatinNC	Phosphate clamp	0.39

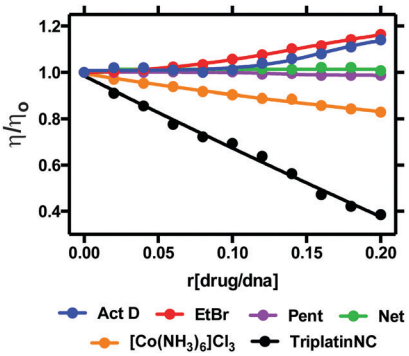

Fig. 7 Relative viscosity values of organic and inorganic compounds bound to duplex stDNA.

3. Spectroscopic techniques

3.1. Absorbance based techniques

Since nucleobases have low symmetry and several heteroatom lone pairs, UV-visible spectroscopy of nucleic acids is dominated by their base absorptions. Transitions for individual bases overlap and produce a single broad strong absorption band for the whole nucleic acid polymer, with an absorbance maximum (A_{max}) between 250–280 nm. The maximal absorbance of nucleic acids (λ_{max}) is dependent on its AT and GC base content. Likewise, the molar extinction coefficient (ε_{max}) of the nucleic acid is dependent on base composition and the preferred secondary structure adopted. A useful resource can be freely accessed on https://www.atdbio.com/tools/oligo-calculator, where the UV and thermodynamic properties of DNA sequences can be calculated.

3.1.1. Thermal melting. Thermal melting (T_M) marks the midpoint in the melting process of DNA, when a 50 : 50 equilibrium exists between helical and single stranded states. Since AT regions contain fewer non-covalent interactions, these hydrogen bonds melt first promoting the initial unwinding of the DNA helix followed by the melting of remaining GC rich regions. The thermal melting process is based on the loss of both hydrophobic interactions and π–π stacking interactions from nearest neighbor interactions due to the denaturation of the double helix and ultimate loss of secondary structure when bases become unstacked. This process is reversible and full renaturation of duplex DNA can occur approximately 25 °C below the denaturation temperature. T_M is a powerful technique that relies on the intrinsic extinction coefficient of nucleic acids and is used to probe the thermodynamic parameters involved in metallodrug–DNA binding interactions.[36]

The differential stability of AT and GC rich regions and splitting of the duplex into single strands, is critical to many cellular processes such as transcription and recombination and is also central to the polymerase chain reaction (PCR). The thermal denaturation of DNA is also strongly influenced by duplex environment including salt and buffered solvent conditions. For example, higher salt concentrations generally result in higher T_M values since the negative charge on the phosphate backbone is diffused due to electrostatic stabilisation. The relationship between T_M and ionic strength can accordingly be exploited to change T_M to a more convenient experimental temperature range.

Thermal denaturation can be easily monitored using a UV-vis spectrophotometer by observing the change in absorbance as a function of temperature. The method offers a useful insight into the strength of drug–DNA interactions as more energy is required to denature the stabilized secondary structure relative to the untreated polynucleotide, the stronger the drug interaction (ΔT_M) and *vice versa*. Since structural factors and base composition impact the affinity of metallodrug–DNA binding this influence can be identified by measuring T_M data. At a basic level, classical measurements involving actinomycin D (intercalator) and netropsin (minor groove binder) with co-polymers poly[d(G–C)$_2$] and poly[d(A–T)$_2$] reveal stabilization factors associated with G–C selective intercalation and A–T dependent minor groove binding (Table 1A). UV melting experiments with alternating copolymers have been applied to study Triplatin complexes and, separately, the influence of intercalating phenazine ligands within Cu-DPQ-Phen and Cu-DPPZ-Phen complexes (Table 1A).[35,37] While alternating co-polymers, and to some extent calf thymus DNA, provide useful binding data, base-selective interactions are highly desirable to identify. Influenced by Cardin and co-workers structural characterisation of selective Λ-[Ru(phen)$_2$(dppz)]$^{2+}$ oligonucleotide (ON)

Table 1 (A) Influence of standard agents and selected copper phenazine complexes on the thermal melting of synthetic alternating copolymers[37] and (B) thermal denaturing of 12-mer duplexes (5 μM) in the presence of Cu-Oda (1.0 loading ratio)[38]

(A)

	ΔT_M (°C)	
Agent	Poly[d(A–T)$_2$]	Poly[d(G–C)$_2$]
Netropsin	12.3 ± 0.8	02.8 ± 0.4
Actinomycin D	−0.3 ± 0.3	12.1 ± 0.9
Cu-DPQ-Phen	0.6 ± 0.2	11.4 ± 1.1
Cu-DPPZ-Phen	0.5 ± 0.1	10.4 ± 1.1

(B)

	ΔT_M (°C)	
Agent	d(GCCGGTACCGGC)$_2$	d(GCCGGATCCGGC)$_2$
Cu-Oda	8.7 ± 1.5	0.8 ± 0.6

binding (Section 2.1.1.), we recently probed the UV-melting of Cu-Oda (Fig. 2B) with palindromic dodecamers containing AT/AT and TA/TA central steps (Table 1B). Sequences with central AT/AT steps were only marginally stabilised whereas the TA/TA step showed significant stabilisation of +8.77 °C and enhanced duplex stability of 4.34 kJ mol^{-1} that we ascribed to selective intercalation.[38]

Method summary	UV thermal melting (indirect)
Requirements	Spectrometer equipped with cell holder containing Peltier heat pumps connected to an external temperature controller. Quartz cuvettes with PTFE stoppers (commonly used).
Results	Thermal melting of phase transitions/molar enthalpy/association constants of metallodrug–nucleic acid interactions.
Advantages	Simple experimental setup. High sensitivity and reproducibility. Suitable for comparing/ranking binding affinity (SAR). Small sample size.
Limitation	Metallodrugs stability/optical transparency at elevated temperatures. Binding information generally provided at non-physiological temperatures (>37 °C).
Complementary and advanced techniques	NMR and viscosity (Sections 2.2 and 2.4) and optical techniques including circular dichroism spectroscopy, indirect fluorometric assays and topoisomerase I-mediated DNA relaxation (Sections 3.1.2, 3.2.1 and 4.2). Advanced complementary techniques include isothermal titration calorimetry (ITC) and qPCR.

3.1.2. Circular dichroism spectroscopy. Circular dichroism (CD) probes the absolute configuration and conformation of a system and is dependent on chirality. UV-vis CD is used extensively for the study of the secondary structure of chiral biomolecules and is particularly useful to determine conformational properties such as the α and β helix of proteins and the A, B and Z-forms of DNA. In the case of DNA, heterocyclic nitrogenous DNA bases are achiral themselves but when linked to a 5′ carbon sugar by a β-glycosidic linkage and placed within the phosphate framework in a stacked helical formation, the molecular secondary structure becomes chiral. Since DNA structures are affected by temperature, pH, and ionic strength, experiments probing drug-induced conformational changes should be carefully designed.[39] Many DNA binding agents are achiral and optically inactive but by observing changes at specific wavelengths in the UV spectrum where DNA typically absorbs (200–320 nm range), it is possible to identify and interpret drug–DNA interactions with extreme sensitivity.[40] The CD profile of right handed B-DNA exhibits two positive (220 nm and 268 nm) and two negative (210 nm and 246 nm) elliptical signals and slight variations arise when the %GC content is varied. CD is typically used to determine the preferred binding mode (*e.g.* minor groove, major groove, intercalation) within the asymmetric DNA environment by observing the CD signal relative to untreated DNA at wavelengths of ~210, 220, 246 and 268 nm (Fig. 8A).

Intercalation of B-DNA typically leads to an increase in the elliptical signal associated with helicity (246 nm) and base pair stacking interactions (268 nm), while minor groove binding agents typically cause a decrease in the elliptical signal associated with hydrogen bonding interactions (220 nm) (Fig. 8B). These interactions can be understood from differences between the action of intercalators where perturbation to the helical backbone is required, and minor groove binders that contract the minor groove due to DNA-adduct H-bonding. The mapping of specific changes to ellipticity as a function of titrated metallodrug is an important approach and was recently applied to identify major groove binding by a novel di-copper(II) complex (Cu_2TPNap); results detailed in Fig. 8B indicate correlation between MG and Cu_2TPNap with subsequent biophysical and computational experiments supporting the interaction.[14] CD can also identify B → Z and B → A conformational changes and the Z transition in poly[d(G–C)$_2$] is shown in Fig. 8C where NaCl was used to stimulate the inversion (unpublished). Poly[d(G–C)$_2$] and poly[d(G)·d(C)] when treated with mono- and bi-functional platinum complexes (including BBR3464). Helical changes associated with condensation (ψ-DNA) may also be monitored and recent evidence of TriplatinNC-mediated DNA condensation using CD spectroscopy were subsequently corroborated by AFM.[15]

An elegant function of CD spectroscopy is its ability to probe sequence-specific metallodrug–ON (oligo) interactions. To gain an understanding of DNA sequence-context to the recognition process of Cu-Oda (Fig. 2B) this approach was applied to palindromic dodecamers with varying AT/AT and TA/TA steps, together with TATA repeats and substituted uracil (*i.e.* UAUA) congeners.[38] Site-specific intercalation (*ca.* 280 nm) at the central TA/TA step in oligo d(GCCGGTACCGGC)$_2$ was identified while a strong Cotton minimum in the same region indicated localized 'Z-like' DNA formation at the central AT/AT step in oligo d(GCCGGATCCGGC)$_2$ (Fig. 8D). Intercalation was also observed in two sequences containing the TATA repeat but when thymine (T) was substituted with uracil (U), the elliptical signal at 288 nm increased suggesting a portion of intercalation occurring at the major groove site with the absence of bulky methyl groups in T rendering the major groove accessible to the di-nuclear complex (Fig. 8D).

CD offers many advantages over NMR and X-ray crystallography in the analysis of structural interactions in biological systems as it is inexpensive and requires small amounts of sample allowing for rapid and highly-sensitive analysis. Linear dichroism—another powerful form of polarized-light spectroscopy complementing CD—has been successfully employed to deduce drug–DNA binding geometries and has been extensively reviewed elsewhere.[41] An additional application of CD spectroscopy, beyond the scope of this tutorial review, is induced circular dichroism (ICD) where wavelength-specific spectral

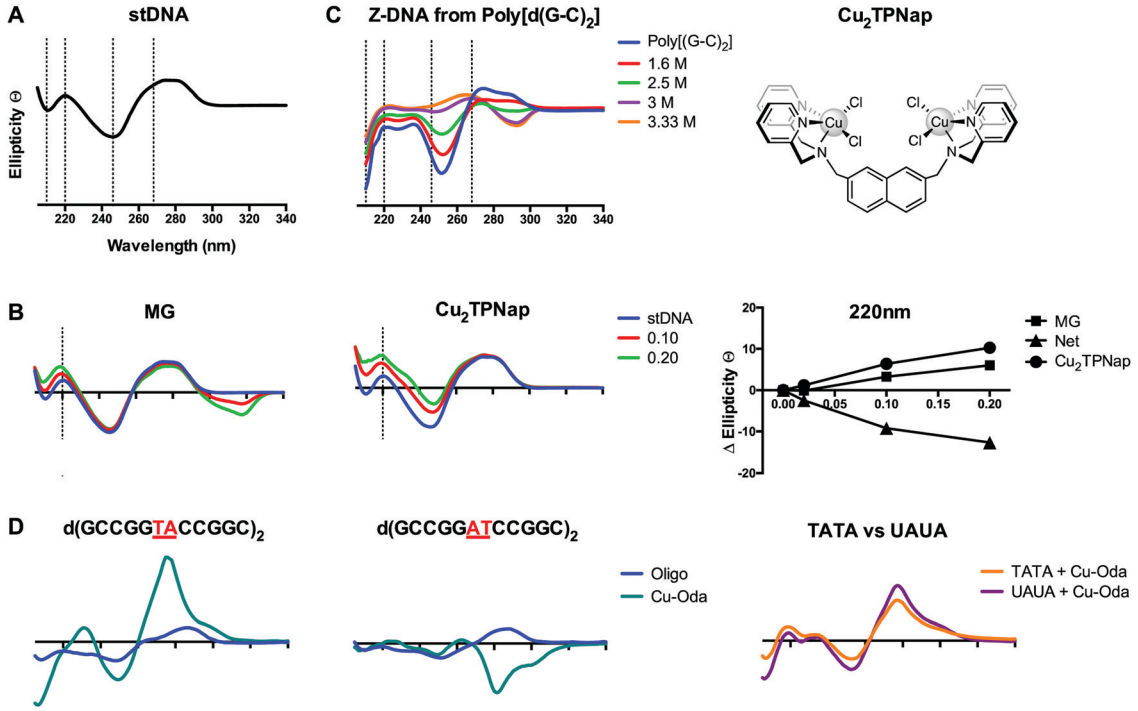

Fig. 8 (A) CD profile of B-form salmon testes DNA (stDNA) highlighting wavelengths of interest including 210, 220, 246 and 268 nm; (B) change in ellipticity of stDNA at 220 nm in the presence increasing ratios of methyl green (MG) and di-nuclear Cu_2TPNap; (C) B → Z NaCl titration of alternating co-polymer poly[d(G–C)$_2$]; and (D) CD spectra of 12mer sequences d(GCCGGTACCGGC)$_2$, d(GCCGGATCCGGC)$_2$ and overlay of d(GCTTTATAAAGC)$_2$ and d(GCUUUAUAAAGC)$_2$ sequences in the presence of Cu-Oda.

changes are measured from coupling of electronic transition moments of the ligand (or complex) and DNA.[40] Finally, care must be taken in the CD analysis of epigenetic bases (*e.g.* formyl-cytosine; fC) as oligomers containing these bases can display non-classical Cotton behavior in the B-form.[42]

Method summary	Circular dichroism (indirect)
Requirements	Circular dichroism spectrometer with continuous nitrogen flow, quartz cuvettes required.
Results	Conformational changes to nucleic acid structure upon metallodrug binding.
Advantages	Excellent sensitivity and reproducibility. Provides structural information related to specific binding interactions. Small sample size.
Limitation	Caution must be taken with chiral metallodrugs. Experimental conditions must carefully maintain DNA structure. Limited solvent choice (UV activity).
Complementary and advanced techniques	Direct binding analysis by UV-vis and fluorescence spectroscopy, DNA unwinding experiments (4.2), and viscosity (2.4). Advanced techniques include linear dichroism along with X-ray crystallography, NMR, UV thermal melting (Sections 2.1, 2.2 and 3.1.1) and molecular dynamics.

3.2. Fluorescence based methods

3.2.1. Indirect fluorometric assays. Fluorogenic organic molecules with high affinity and binding selectivity to nucleic acids are invaluable tools in molecular and chemical biology. They are particularly helpful to probe the indirect DNA binding affinity of metallodrugs with low molar extinction coefficients (*e.g.* Cu(II), Pt(II), and Mn(II)) where direct spectroscopic measurements are precluded. Examples of such dyes routinely used in fluorescence microscopy and flow cytometry include the blue fluorescent AT-specific minor groove binder DAPI (4′,6-diamidino-2-phenylindole, Fig. 2E), commonly used as a nuclear counterstain; intercalating Sybr Green I, used for the detection of double and single stranded DNA and also as a chromosomal stain; and the red fluorescent nuclear and chromosome counterstain, propidium iodide (3,8-diamino-5-[3-(diethylmethylammonio)-propyl]-6-phenylphenanthridinium diiodide) (Fig. 2G). Fluorescent dyes, however, are not just limited to microscope imaging. They are applied in high-throughput assays designed to indirectly assess the affinity with which a small drug molecule binds to DNA and in more sophisticated analysis involving fluorescence resonance energy transfer (FRET) assays. Two examples of fluorophores for measurement of duplex DNA binding affinity the planar heterocyclic intercalator, ethidium bromide (3,8-diamino-5-ethyl-6-phenylphenanthridinium bromide; EtBr, Fig. 2G), and the crescent shaped minor groove binding agent Hoechst 33258 (Fig. 2E). Since these molecules have low fluorescence in solution and become highly fluorescent once bound to DNA, their photophysical properties can be used to determine

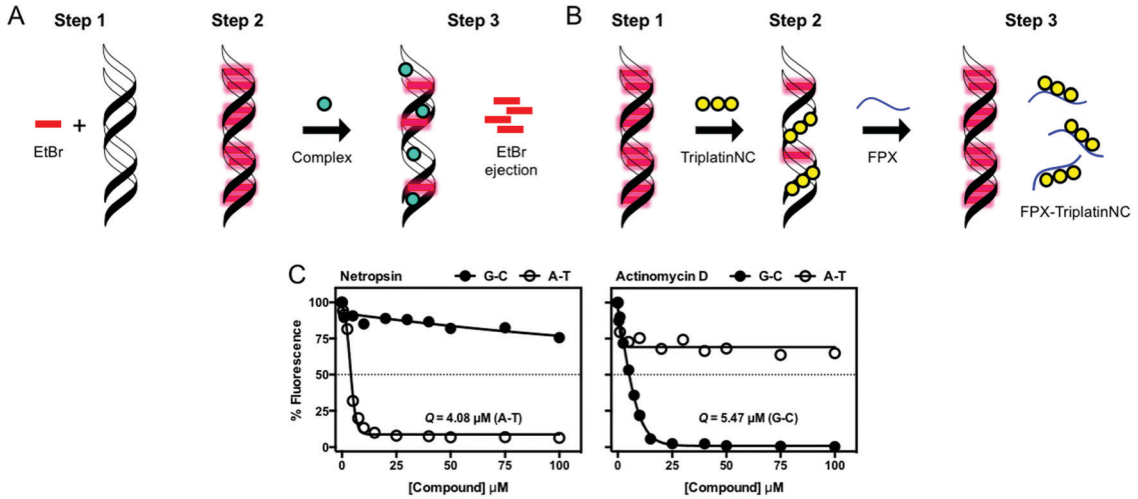

Fig. 9 (A) Indirect fluorescence displacement assay using ethidium bromide as a reporter molecule to determine apparent binding constants (K_{app}) of non-fluorescent DNA-binding agents; (B) FPX-TriPtNC binding assessment assay; and (C) fluorescence quenching of limited bound intercalator (EtBr) to poly[d(G–C)$_2$] and poly[d(A–T)$_2$] upon titration of netropsin and actinomycin D. Reproduced from ref. 37 with permission from the American Chemical Society, copyright 2014.

the ability of metallodrugs to bind DNA through depletion of fluorescence intensity.

3.2.2. Competitive fluorescent displacement. The competitive EtBr displacement assay is an indirect titration technique used to determine the apparent binding constants (K_{app}) of non-fluorescent DNA-binding ligands and complexes (Fig. 9A). This use of the intercalator EtBr to probe drug–DNA binding constants was originally proposed in 1979 by Morgan *et al.*[43] and carried out in rectangular quartz cuvettes, however in recent years we have modified this assay to take advantage of a 96-well fluorescence plate reader to allow for high-throughput metallodrug binding analysis.[37] This procedure involves treating DNA (10 μM) with an excess of the intercalating ethidium bromide molecule (12.6 μM) to saturate all available binding sites which results in strong fluorescence. This quantitative titration method is then used to determine the amount of test sample required to induce a 50% decrease in the fluorescence of the EtBr reporter molecule, referred to as the C_{50} value. Using this high-throughput approach, drug concentrations are measured in triplicate and the apparent binding constants are calculated using $K_{app} = K_e \times 12.6/C_{50}$ where $K_e = 8.8 \times 10^6$ M(bp)$^{-1}$. This reproducible displacement assay can be applied to rank the binding affinity of both individual and families of structurally related compounds over a defined concentration range.[35,37] Recently, this displacement assay was elegantly adapted to assess TriplatinNC–DNA binding interactions with the highly sulfated pentasaccharide Fondaparinux (FPX) as illustrated in Fig. 9B. Bound TriplatinNC was sequestered from DNA using equimolar concentrations of the model heperan sulfate (HS)-like substrate FPX indicating that FPX sulfate clusters have high binding affinity for PPCs. This assessment was made on the basis of the reappearance of fluorescence from EtBr reporter molecules intercalating DNA free from bound TriplatinNC.[15]

3.2.3. Competitive fluorescence quenching. Fluorescence quenching assays under conditions of excess DNA (*e.g.* 25 μM M(bp)$^{-1}$) treated with limited bound fluorophore (*e.g.* 5 μM) permits identification of preferential DNA binding sites. This method is quite different to saturated binding (*i.e.* competition binding) and may be performed at pH 5.0 to ensure binding agents are present chiefly in their protonated form. Not only can fluorescent probe molecules be varied based on their mode of interaction (*e.g.* EtBr – intercalator; Hoechst 33258 – minor groove binder) but so too can the duplex DNA target.[37] Data is presented as quenching (Q) values that are defined as the concentration of test sample required to induce 50% quenching of drug-free control fluorescence. The technique is particularly useful when comparing Q values within structurally-related metallodrug families and within oligomers of varying sequence context (Fig. 9C shows exemplary data from classical agents).

Method summary	Fluorescence reporting (indirect)
Requirements	Fluorescence spectrophotometer and quartz cuvette or fluorescence plate reader for high throughput analysis and suitable fluorescent reporter dyes.
Results	Indirect evidence of DNA binding when combined with specific reporter dyes. Binding constant can be obtained for compounds lacking a chromophore.
Advantages	High-throughput analysis possible when combined with 96 well plates.
Limitation	Indirect method with a reliance on signal from a fluorogenic reporter. Quenching of the reporter by metallodrug must be examined prior to analysis.
Complementary and advanced techniques	NMR, mass spectrometry and viscosity (Sections 2.2, 2.3, and 2.4) and optical techniques including thermal melting and circular dichroism (Sections 3.1.1 and 3.1.2). Advanced techniques include surface plasmon resonance (SPR) and molecular dynamics.

4. Electrophoretic-based techniques

4.1. An introduction to gel mobility shift assays

Electrophoretic gel mobility shift assays are a well-established analytical technique used to analyze, separate and purify nucleic acid samples. Gel electrophoresis involves the movement of DNA through a solid-phase sieve-like medium such as agarose or polyacrylamide, under the influence of an electric potential difference. Due to its inherent negative charge, DNA moves in the electric field as an anion, from the cathode to the anode. The rate of DNA migration through the gel is dependent on several factors including the length of the DNA sequence and its conformation. Thus, long DNA fragments migrate slower than shorter fragments through an agarose medium as they experience greater resistance when travelling through a matrix of small pores within the gel. A number of external parameters can be controlled in order to maximize the resolution of a gel including the agarose content, its physical length, and the voltage applied allied with running time. Another important aspect of gel electrophoresis is the study of plasmid DNA vectors. These vectors are isolated from bacteria and are generally found in a supercoiled (SC) state. Manipulation of SC plasmid DNA by endonucleases or damaging agents gives rise to open-circular (OC) and linear (L) isoforms (Fig. 10A). Since supercoiled DNA is tightly compacted and has a small mass-to-charge ratio, it migrates with ease through an agarose medium. Once the plasmid becomes nicked on a single strand (*i.e.* single strand break (SSB) induction), supercoils become released resulting in the formation of open-circular DNA which experiences more resistance due to its larger size in the agarose matrix. Linear DNA results from double strand breaks (DSBs) and clustered DNA damage and this form experiences less resistance than open-circular DNA during its migration through an agarose medium (Fig. 10A). Metallodrug–DNA damage can therefore be identified using plasmid DNA and the rate of conversion between SSB and DSBs estimated by band densitometry.

4.2. Superhelical DNA unwinding and topoisomerase I-mediated relaxation

Electrophoretic mobility shift assays can be employed to determine the influence of covalent drug interactions on DNA supercoiling. The terms that need to be considered when discussing topological constraint stem from the formula Lk = $T + W$, where Lk = linking number, Tw = twist (number of helical turns of the DNA duplex) and Wr = writhe (number of supercoils). This technique has previously been used to investigate a series of structurally related Pt(II) complexes that differed in their covalent

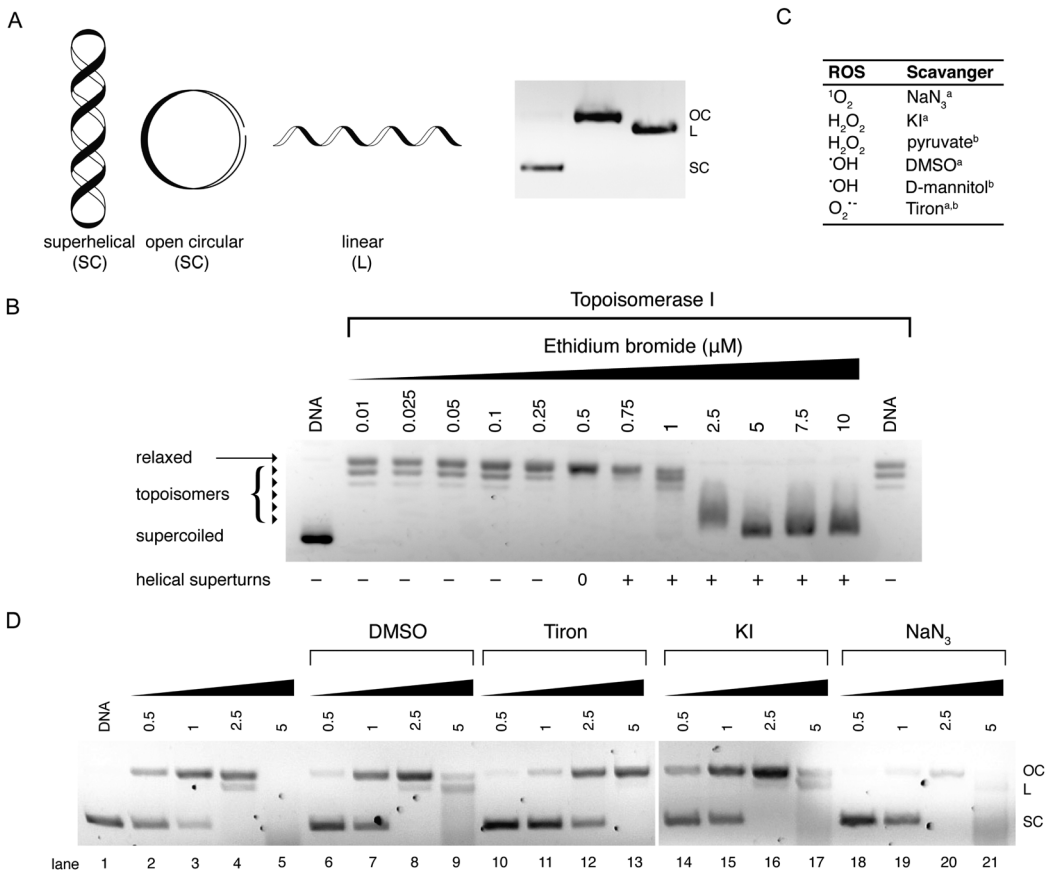

Fig. 10 (A) Cartoon illustration of superhelical (SC), open circular (OC) and linear (L) DNA and agarose gel electrophoresis representation of respective DNA forms; (B) topoisomerase I mediated DNA relaxation assay in the presence of intercalating agent EtBr; (C) table of selected free radical scavengers[a] and intracellular antioxidants[b]; and (D) gel profile of plasmid DNA treated with Cu-Ph-Phen in the absence (lanes 2–5) and presence of radical-specific antioxidants and trapping agents (lanes 6–21). Reproduced from ref. 50 with permission from the American Chemical Society, copyright 2016.

co-ordination mode (mono-functional/bi-functional).[44] In the presence of increasing concentrations of a covalent binding small molecule, the migration rate of SC–DNA is monitored. When all supercoils are removed from the plasmid—due to crosslinking or intercalation—the migration pattern of DNA is identical to that of OC–DNA. The bound drug-to-nucleotide ratio at this point can be visualised in the agarose gel and referred to as the coalescence point. When the drug loading ratio is further increased beyond this point, positive supercoiling can be detected as the plasmid becomes wound in the opposite direction under the influence of excess metallodrug/intercalator.

Another method to reliably identify DNA intercalation is *via* topoisomerase I-mediated DNA relaxation. Topoisomerases (Topo) are a specialised class of nuclear enzymes that catalyse the transient cleavage, manipulation and resealing of either a single strand (Topo I) or double strand (Topo II) of DNA. This activity allows the relaxation of chain intertwinement and the release of superhelical tension to permit topological changes required during replication, transcription, and DNA repair.[45] Topo I-mediated relaxation is a robust assay to identify intercalative properties of suspect DNA binding metallodrugs. Complexes with intercalating moieties, typically constructed from planar aromatic ligands, unwind and elongate the helical structure inhibiting topoisomerase enzymes from binding to DNA, or alternatively stabilising the enzyme–DNA complex.

Topo I isolated from *E. coli* relaxes negatively coiled superhelical plasmid DNA giving a distinct topological pattern of negative, or right handed, topoisomers (Fig. 10B). In the presence of intercalating agent EtBr, plasmid DNA becomes unwound and transitions from its negatively wound topological pattern to fully relaxed OC DNA, and then to positively (left-handed) SC plasmid as the plasmid becomes wound in the opposite direction.[46] This unwinding effect is evident in lanes 2–14 of Fig. 10B where EtBr induces helical unwinding by 26°, with positively wound topology of scDNA becoming visible after 0.5 μM exposure. The distinct "up and down" migration pattern evident in Fig. 10B is a typical trend observed when SC plasmid DNA is treated with an intercalating agent. As the concentration of the bound intercalant increases, negatively charged SC DNA becomes unwound forming relaxed OC DNA which migrates slower through the agarose medium than tightly packed SC DNA. When the concentration of the intercalant is further increased, OC DNA is wound tightly in the opposite direction forming positively charged SC DNA that migrates at a similar rate to negatively charged SC DNA.

4.3. Oxidative DNA damage detection DNA damage

4.3.1. Introduction to DNA oxidation. DNA damage is known to play a major role in biological processes including ageing, mutagenesis and carcinogenesis as cellular DNA is susceptible to many forms of damage resulting from exposure to endogenous (spontaneous) and exogenous (environmental) sources. Examples of endogenous factors include enzymatic or spontaneous metabolic conversions, while exogenous sources include genotoxic agents such as ionizing radiation, redox metal ion overload, and therapeutic metallodrug exposure. Such mutagens are capable of causing direct or indirect damage to nucleotides and result in profound biological consequences including replication errors in genetic code and the production of oxidative DNA base lesions. Two major types of DNA damage mechanisms exist, hydrolytic and oxidative. Hydrolytic agents cause cleavage of the phosphate backbone which can be enzymatically repaired by DNA ligases, while oxidative mechanisms involve the production of diffusible free radicals resulting in DNA cleavage by oxidative attack at a variety of C–H positions of the deoxyribose moiety.[47]

4.3.2. Artificial chemical nuclease activity. The discovery of the first synthetic chemical nuclease Cu-Phen (Fig. 2A) sparked intensive effort toward the development of new artificial metallonucleases.[48] There are, however, numerous limitations associated with Cu-Phen including (i) binding to both nucleic acids and proteins without specificity thereby inducing general cytotoxicity, (ii) a high dissociation constant of the second coordinated phenantholine ligand and (iii) a dependence on the presence of a reductant (*e.g.* L-ascorbic acid) and an oxidant (O_2 or H_2O_2) required to activate a cascade of redox reactions mediated by the reduction of Cu(II) to Cu(I).

Our efforts to develop this metallodrug class have focused on the incorporation of designer DNA intercalating ligands such as DPPZ and also on the role of nuclearity. One recent study involved the isolation of ternary Cu(II) complexes incorporating both 1,10-phenathroline and phenazine ligands; through the systematic extension of the ligated phenazine ligand in the Cu^{2+} bis-phenanthroline model, it was possible to enhance the chemical nuclease profile of the series relative to Cu-Phen where the activity trend Cu-DPQ-Phen ≈ Cu-DPPZ-Phen > CuPhen (Fig. 2) was observed.[37] Reactive oxygen species (ROS) responsible for oxidative DNA damage by this series were later investigated using superhelical plasmid DNA with a selection of ROS-specific anti-oxidants and stabilisers as follows: NaN_3 for singlet oxygen ($^1O_2$); KI for hydrogen peroxide (H_2O_2); DMSO for the hydroxyl radical ($^{\bullet}OH$); and D_2O for stabilising singlet oxygen ($^1O_2$) (Fig. 10C). Experiments revealed the hydroxyl radical as chiefly responsible for degradation.[49] Recently, this method was extended to examine the *in vitro* and intracellular cleavage efficacy of the developmental therapeutic [Cu(*o*-phthalate)(1,10-phenanthroline)] (Cu-Ph-Phen, Fig. 2C) and results are shown in Fig. 10D.[50] Experiments here revealed superoxide ($O_2^{\bullet -}$) as a prominent species responsible for DNA oxidation as co-incubation with 4,5-dihydroxy-1,3-benzene-disulfonic acid (tiron) significantly impeded DNA damage and prevented double strand damage (lane 10–13). The presence of DMSO diminished activity to a lesser extent while DNA damage was only marginally altered by KI (lane 14–17) and NaN_3 (lane 18–21). Significantly, in the same study ovarian adenocarcinoma cancer cells (SKOV3) pretreated with tiron and subsequently exposed to an LD_{50} concentration of Cu-Ph-Phen displayed enhanced survival by ~26%.[50] A further example showing correlation between ROS mediators of *in vitro* DNA damage and cell culture cytotoxicity can be found in ref. 38.

Oxidative DNA damage is known to be dependent on a number of factors including and not limited to: DNA plasmid type and conformation, presence/absence of exogenous oxidant and reductant, presence of chelating agents and dependence on hydrogen peroxide. The presence of non-covalent recognition

elements such as minor groove (netropsin), major groove (methyl green) and electrostatic agents ($[Co(NH_3)_6]Cl_3$) can influence accessibility for DNA damaging drugs. Analysis of plasmid DNA cleavage involving the copper(II) phenazine series (Cu-Phen-DPQ; Cu-Phen-DPPZ; and Cu-Phen-DPPN) with pre-incubation of the major groove binding agent methyl green (Fig. 2F) resulted in enhanced chemical nuclease activity, indicative of drug–DNA interactions being directed towards the minor groove, while the presence of the minor groove binding agent netropsin was found to reduce the oxidative DNA damage profile of the same complex series.[49]

4.4. Melphalan protection assay

To establish the minor groove as a preferred drug–DNA binding site the aromatic nitrogen mustard melphalan can be employed. When in solution, the bis(2-chloroethyl)amino side chain of the molecule can cyclize to form the aziridinium ion which can add to a nucleophilic site on DNA forming a mono-alkylated covalent DNA adduct. This process can be repeated to form a di-alkylated adduct resulting in intra- or inter-strand crosslinking between two complementary strands of DNA. Subsequent heat-treatment with piperidine induces thermolabile DNA cleavage at guanine N7 (major groove) and adenine N3 (minor groove) sites (Fig. 11B). When DNA is pretreated with cationic minor groove binding agents such as netropsin or distamycin, these molecules afford protection to DNA from the alkylation process by occupying the narrow AT-rich minor groove and prevent thermolabile scission from occurring. Interestingly, the same protective effects can be seen in the case of PPCs and classical minor groove binders, where melphalan is prevented from accessing A-rich regions in the minor groove and this protective effect is outlined in Fig. 11C.[14,29]

Method summary	Agarose gel electrophoresis (indirect)
Requirements	Gel electrophoresis tank, power pack, transilluminator, agarose, plasmid DNA and DNA specific stain. DNA/RNA ladders necessary for accurate sizing.
Results	DNA damage and stepwise conversion of SC → OC → LC. Also possible to determine conformational changes to nucleic acid structure upon metallodrug binding.
Advantages	Simple experimental setup, cost effective, small sample size. Fast analysis time.
Limitation	Quantitation of DNA damage/modification (with densitometry, for example) relies on reporters (indirect) that bind conformers at different ratios.
Complementary and advanced techniques	Polyacrylamide gel electrophoresis (PAGE), Mass spectrometry and on-chip microfluidics (Sections 2.3 and 4.5). Advanced techniques include qPCR and LC-MS/MS stable isotope dilution detection for DNA damage, and 8-oxo-dG ELISA detection.

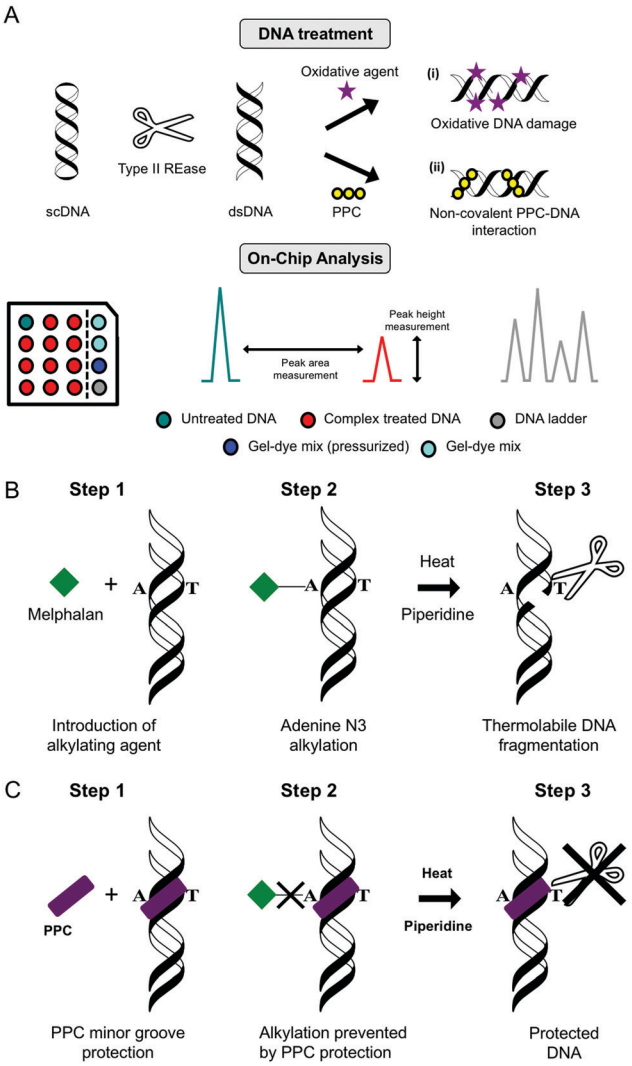

Fig. 11 (A) Double stranded DNA "on-chip" protocol developed within our research laboratories used to assess (i) oxidative DNA damage and (ii) PPC non-covalent binding interactions using the Agilent BioAnalyser 2100 platform; (B) melphalan alkylation assay using piperidine and heat to induce thermolabbile scission and (C) minor groove protection assay polynuclear platinum complexes (PPC).

4.5. On-chip microfluidics

Lab on chip technology (*e.g.* the Agilent Bioanalyser 2100) has provided a platform to conduct high-throughput gel electrophoretic experiments on a microfluidic chip with up to 12 DNA, RNA or protein samples being analyzed and processed sequentially. There are many advantages to the method including broad sample size range (25–12 000 bp), minimal sample consumption and high sizing resolution with accuracy normalised to internal reference markers. Data can be processed and generated with output including electrograms, peak height, peak area and digital electropherograms. Many applications for nucleic acids have been found for this technique including determination of sample size, quality and concentration (Fig. 11A).

Recently, we employed this technique to determine drug–DNA damage and selective binding interactions with double

stranded DNA sequences. In the first case, an assay was devised to compare the oxidative degradation profiles of a family of structurally related bis-chelate Cu(II) complexes of Cu-DPQ-Phen, Cu-DPPZ-Phen, and Cu-DPPN-Phen on restricted pUC19. By employing both peak height and area it was possible to rank the fragmentation activity of the complex series with Cu-DPQ-Phen identified as the most active agent.[37] In another application of this technique, cationic Triplatin complexes of varying linker length $[\{trans\text{-}Pt(NH_3)_2(NH_2(CH_2)_nNH_3)\}_2\text{-}\mu\text{-}(\{trans\text{-}Pt(NH_3)_2(NH_2(CH_2)_nNH_2)_2\}\})](NO_3)_8$, where n = 5 (AH78P), 6 (AH78 TriplatinNC) and 7 (AH78H) were determined to inhibit site-selective excision by type II restriction endonucleases—a consequence of which might indicate their ability to negate native DNA excision repair processes. The experimental setup involved pre-incubating DNA with PPC complexes followed by endonuclease exposure to BamHI, EcoRI, and SalI. Concentration dependent inhibition was identified in many cases, with high intensities of the native pUC19 band becoming visible.[35] Additionally, the technique identified how PPC linker chain length modulates endonuclease access to the restriction sites. In this work, the pentanediamine complex (n = 5) protected or inhibited digestion in the nanomolar range, while a 10-fold increase was required to block restriction activity in the hexane- (n = 6) and heptane-bridged (n = 7) congeners.

Method summary	On-chip microfluidics (indirect)
Requirements	Commercially available microfluidic systems such as the Agilent Bio-Analyser and preferred chip types (*e.g.* DNA 1000, DNA 7500).
Results	Output from this technique includes electropherograms, electrograms, and advanced analysis including %DNA degradation.
Advantages	Quantitative method with high sizing resolution. Accuracy of individual chips is normalised to internal reference markers. Experiments can be optimised using inexpensive agarose methods.
Limitation	Expense, scaling between DNA sizes requires change of microfluidic chip, can be analytically challenging.
Complementary techniques	Mass spectrometry analysis (Section 2.3).

5. Conclusion

DNA is a well-established pharmacological target for metallodrugs and developmental anticancer complexes continue to be rationally designed for potential clinical use against this target. The elucidation of non-covalent binding modes, along with helical and groove residency is a crucial area of study in this field. This tutorial review has focused on selected molecular methods for investigating metallodrug–DNA interactions using gel electrophoretic, electronic and fluorescent spectroscopic, NMR spectroscopic, X-ray crystallographic and mass spectrometric techniques. Significantly, when combinations of complementary molecular methods are employed, the full picture of solution binding properties can be defined, which ultimately broaden our understanding of complex-DNA binding. Recent work on probing the nucleic acid binding mode by 'phosphate clamping' Triplatin complexes elegantly reveals how these molecular techniques function synergistically.[35] Using a family of cationic tri-platinum(II) complexes of varying aliphatic linker length $[\{trans\text{-}Pt(NH_3)_2(NH_2(CH_2)_nNH_3)\}_2\text{-}\mu\text{-}(\{trans\text{-}Pt(NH_3)_2(NH_2(CH_2)_nNH_2)_2\}\})](NO_3)_8$, where n = 5 (AH78P), 6 (AH78; TriplatinNC) and 7 (AH78H), high-affinity PPC–DNA interactions were uncovered using ethidium bromide fluorescence quenching, while cooperative fluorescence binding of Hoechst 33258 was observed at the minor groove. Conformational changes on long DNA were then identified using viscosity, electrophoretic, and CD spectroscopic methods where aggregation/condensation of nucleic acids was evidenced in tandem with conversion from B → Z-DNA. 2D-^{1}H NMR experiments, in conjunction with several other molecular methods, then indicated two limiting modes of phosphate clamping—backbone tracking (GC dependent) and groove spanning (AT dependent)—could be distinguished and implied DNA condensation was driven, primarily, by minor-groove spanning. Further application of electrophoresis (including 'on-chip' microfluidics) showed Triplatin–DNA binding prevented endonuclease activity by type II restriction enzymes. Subsequent work by Farrell and co-workers identified nucleolar condensation in colorectal cancer cells using confocal microscopy with atomic force microscopy (AFM) studies showing this class to condense both tRNA and duplex DNA structures.[15] Other examples on the application of molecular methods have been described in this review and, with this in mind, the overlap and versatility of complementary techniques can augment our understanding of non-covalent metallodrug–DNA interactions.

Conflicts of interest

There are no conflicts to declare.

Acknowledgements

This work was supported by Science Foundation Ireland (15/CDA/3648). AK acknowledges support from the Marie Skłodowska-Curie Innovative Training Network (ITN) ClickGene (H2020-MSCA-ITN-2014-642023). NF acknowledges support by NIH RO1CA78754.

References

1 N. P. E. Barry and P. J. Sadler, *Chem. Commun.*, 2013, **49**, 5106–5131.
2 E. Chargaff, *Science*, 1971, **172**, 637–642.
3 R. Wing, H. Drew, T. Takano, C. Broka, S. Tanaka, K. Itakura and R. E. Dickerson, *Nature*, 1980, **287**, 755–758.

4 A. Rich and S. Zhang, *Nat. Rev. Genet.*, 2003, **4**, 566–572.
5 H. R. Drew and R. E. Dickerson, *J. Mol. Biol.*, 1981, **152**, 723–736.
6 R. E. Dickerson, H. R. Drew, B. N. Conner, R. M. Wing, A. V. Fratini and M. L. Kopka, *Science, New Series*, 1982, **216**, 475–485.
7 M. Zeraati, D. B. Langley, P. Schofield, A. L. Moye, R. Rouet, W. E. Hughes, T. M. Bryan, M. E. Dinger and D. Christ, *Nat. Chem.*, 2018, **10**, 631–637.
8 G. Biffi, D. Tannahill, J. McCafferty and S. Balasubramanian, *Nat. Chem.*, 2013, **5**, 182–186.
9 C. Hiort, P. Lincoln and B. Nordén, *J. Am. Chem. Soc.*, 1993, **115**, 3448–3454.
10 C. J. Cardin and J. P. Hall, in *DNA-targeting Molecules as Therapeutic Agents*, ed. M. J. Waring, Royal Society of Chemistry, Cambridge, 2018, pp. 198–227.
11 H. Song, J. T. Kaiser and J. K. Barton, *Nat. Chem.*, 2012, **4**, 615–620.
12 J. K. Barton, A. N. Boynton and K. M. Boyle, in *DNA-targeting Molecules as Therapeutic Agents*, ed. M. J. Waring, Royal Society of Chemistry, Cambridge, 2018, pp. 367–390.
13 A. Oleksi, A. G. Blanco, R. Boer, I. Usón, J. Aymamí, A. Rodger, M. J. Hannon and M. Coll, *Angew. Chem., Int. Ed.*, 2006, **118**, 1249–1253.
14 Z. Molphy, D. Montagner, S. S. Bhat, C. Slator, C. Long, A. Erxleben and A. Kellett, *Nucleic Acids Res.*, 2018, **46**, 9918–9931.
15 N. P. Farrell, *Chem. Soc. Rev.*, 2015, **44**, 8773–8785.
16 T. C. Jenkins, in *Drug–DNA Interaction Protocols*, ed. K. R. Fox, Totowa, NJ, 1st edn, 1997, vol. 90, pp. 195–218.
17 S. K. Kim and B. Nordén, *FEBS Lett.*, 1993, **315**, 61–64.
18 P. Lincoln, L. M. Wilhelmsson and B. Nordén, in *DNA-targeting Molecules as Therapeutic Agents*, ed. M. J. Waring, Royal Society of Chemistry, Cambridge, 2018, pp. 45–73.
19 R. E. Franklin and R. G. Gosling, *Nature*, 1953, **171**, 740–741.
20 P. M. Takahara, A. C. Rosenzweig, C. A. Frederick and S. J. Lippard, *Nature*, 1995, **377**, 649–652.
21 E. F. Garman, *Science*, 2014, **343**, 1102–1108.
22 J. R. Helliwell and E. P. Mitchell, *IUCrJ*, 2015, **2**, 283–291.
23 L. S. Lerman, *J. Mol. Biol.*, 1961, **3**, 18–30.
24 R. Galindo-Murillo, J. C. García-Ramos, L. Ruiz-Azuara, T. E. Cheatham and F. Cortés-Guzmán, *Nucleic Acids Res.*, 2015, **43**, 5364–5376.
25 P. J. Bond, R. Langridge, K. W. Jennette and S. J. Lippard, *PNAS*, 1975, **72**, 4825–4829.
26 M. Howe-Grant and S. J. Lippard, *Biochemistry*, 1979, **18**, 5762–5769.
27 S. Komeda, T. Moulaei, K. K. Woods, M. Chikuma, N. P. Farrell and L. D. Williams, *J. Am. Chem. Soc.*, 2006, **128**, 16092–16103.
28 M. J. Hannon, *Chem. Soc. Rev.*, 2007, **36**, 280–295.
29 S. Komeda, Y. Qu, J. B. Mangrum, A. Hegmans, L. D. Williams and N. P. Farrell, *Inorg. Chim. Acta*, 2016, **452**, 25–33.
30 S. J. Berners-Price, L. Ronconi and P. J. Sadler, *Prog. Nucl. Magn. Reson. Spectrosc.*, 2006, **49**, 65–98.
31 J. J. Moniodis, D. S. Thomas, M. S. Davies, S. J. Berners-Price and N. P. Farrell, *Dalton Trans.*, 2015, **44**, 3583–3593.
32 Y. Qu, R. G. Kipping and N. P. Farrell, *Dalton Trans.*, 2015, **44**, 3563–3572.
33 T. Urathamakul, D. J. Waller, J. L. Beck, J. R. Aldrich-Wright and S. F. Ralph, *Inorg. Chem.*, 2008, **47**, 6621–6632.
34 J. B. Mangrum and N. P. Farrell, *Chem. Commun.*, 2010, **46**, 6640–6650.
35 A. Prisecaru, Z. Molphy, R. G. Kipping, E. J. Peterson, Y. Qu, A. Kellett and N. P. Farrell, *Nucleic Acids Res.*, 2014, **42**, 13474–13487.
36 J. B. Chaires, in *DNA-targeting Molecules as Therapeutic Agents*, ed. M. J. Waring, Royal Society of Chemistry, Cambridge, 2018, pp. 74–95.
37 Z. Molphy, A. Prisecaru, C. Slator, N. Barron, M. McCann, J. Colleran, D. Chandran, N. Gathergood and A. Kellett, *Inorg. Chem.*, 2014, **53**, 5392–5404.
38 C. Slator, Z. Molphy, V. McKee, C. Long, T. Brown and A. Kellett, *Nucleic Acids Res.*, 2018, **46**, 2733–2750.
39 G. R. Bishop and J. B. Chaires, *Curr. Protoc. Nucleic Acid Chem.*, 2002, **11**, 7.11.1–7.11.8.
40 N. C. Garbett, P. A. Ragazzon and J. B. Chaires, *Nat. Protoc.*, 2007, **2**, 3166–3172.
41 B. Nordén, F. Tjerneld and E. Palm, *Biophys. Chem.*, 1978, **8**, 1–15.
42 J. S. Hardwick, D. Ptchelkine, A. H. El-Sagheer, I. Tear, D. Singleton, S. E. V. Phillips, A. N. Lane and T. Brown, *Nat. Struct. Mol. Biol.*, 2017, **24**, 544–552.
43 A. R. Morgan, J. S. Lee, D. E. Pulleyblank, N. L. Murray and D. H. Evans, *Nucleic Acids Res.*, 1979, **7**, 547–569.
44 M. V. Keck and S. J. Lippard, *J. Am. Chem. Soc.*, 1992, **114**, 3386–3390.
45 J. C. Wang, *Nat. Rev. Mol. Cell Biol.*, 2002, **3**, 430–440.
46 P. Peixoto, C. Bailly and M.-H. David-Cordonnier, in *Drug–DNA Interaction Protocols*, ed. K. R. Fox, Humana Press, 2nd edn, 2010, vol. 613, pp. 235–256.
47 M. Pitié and G. Pratviel, *Chem. Rev.*, 2010, **110**, 1018–1059.
48 D. S. Sigman, A. Mazumder and D. M. Perrin, *Chem. Rev.*, 1993, **93**, 2295–2316.
49 Z. Molphy, C. Slator, C. Chatgilialoglu and A. Kellett, *Front. Chem.*, 2015, **3**, 1–9.
50 C. Slator, N. Barron, O. Howe and A. Kellett, *ACS Chem. Biol.*, 2016, **11**, 159–171.

